

1 **Modeling analysis of the seasonal characteristics of haze formation in** 2 **Beijing**

3 X. Han¹, M. Zhang^{1,*}, J. Gao², S. Wang², and F. Chai²

4 ¹ State Key Laboratory of Atmospheric Boundary Layer Physics and Atmospheric Chemistry, Institute of
5 Atmospheric Physics, Chinese Academy of Sciences, HuaYanBeiLi 40#, Chaoyang District, Beijing
6 100029, China

7 ² Chinese Research Academy of Environmental Sciences, Beijing 100012, China

8
9 *Correspondence to:* M. Zhang (mgzhang@mail.iap.ac.cn)

10
11 **Abstract.** The air quality modeling system RAMS-CMAQ coupled with an aerosol optical property
12 scheme was applied to simulate the meteorological field, major aerosol components (sulfate, nitrate,
13 ammonium, black carbon, organic carbon, dust, and sea salt), and surface visibility over the North China
14 Plain (NCP) in 2011. The modeled results in February and July 2011 were selected and analyzed to obtain
15 an in-depth understanding of the haze formation mechanism in Beijing in different seasons. The
16 simulation results showed that the visibility below 10 km covered most regions of NCP and dropped
17 below 5 km over Beijing and Tianjin megacities, the whole area of Hebei province, and northwest part of
18 Shandong province during the pollution episodes in February and July. The heavy mass concentration of
19 PM_{2.5} ranged from 120 $\mu\text{g m}^{-3}$ to 300 $\mu\text{g m}^{-3}$ was concentrated in the same areas as well. The haze
20 formation mechanism in Beijing in winter was obviously different from that in summer. The mass
21 concentration of PM_{2.5} was relatively higher and the components were complicated in winter. While the
22 mass concentration of PM_{2.5} in summer was relatively lower than that in winter, but the mass
23 concentrations of hygroscopic inorganic salts were comparable with those in winter and the relative
24 humidity was obviously higher. Therefore, the water uptake of hygroscopic aerosols played a key role in
25 summer. Moreover, the analysis shows that the influence of PM_{2.5} mass burden on visibility is very weak
26 when its value located in a high level (larger than 100 $\mu\text{g m}^{-3}$). Only when the mass burden of PM_{2.5}
27 decreases to a certain threshold interval can the visibility increase rapidly. This indicates that when
28 emission reduction measures are taken to control haze occurrence, the mass burden of PM_{2.5} must be cut
29 down below this certain threshold interval. The relationship between threshold of haze occurrence and

relative humidity in Beijing was fitted by the exponential function, and the fitting curves could be a new theoretical basis for the further understanding and control of the haze formation in Beijing.

1. Introduction

The emissions of air pollutants have recently increased significantly because of the economic growth, rapid population expansion, and urbanization in the North China Plain (NCP). Beijing, which is the capital of P. R. China, has a population of over 20 million and is the political, economic, and cultural center of China. This megacity is located at the northern tip of NCP and surrounded by high mountains in its northern and western boundaries. Beijing has suffered from air quality deterioration in the past decade because of strong local emissions (Sun et al., 2006) and long-range transport from the surrounding urban areas (Zhang et al., 2012) located in the east and south of NCP; such areas include Tianjin, Shijiazhuang, and a number of cities where the economic development is most active in Hebei Province. The air pollution in Beijing is easily aggravated by its special geographic position when stable weather appears or the south wind dominates. Although the SO₂ emission in Beijing in the last five years has been decreased by various measures prescribed by the current legislation on emission controls (Lu et al., 2010; Zhang et al., 2006), the mass burden of particulate pollutants remains at a high level (Hao et al., 2013; Zhang et al., 2013), causing serious environmental issues and associated health effects.

Atmospheric haze is caused by the visibility deterioration (lower than 10 km when the relative humidity does not higher than 90%, Wu et al., 2007) through light extinction by aerosol particles. As a result of the high level of aerosol loadings, widespread haze cloud caused by serious air pollution occurred more frequently over this region in the past decade (Ma et al., 2010; Tao et al., 2012; Wang et al., 2013; Zhao, et al., 2011). A number of studies have investigated the long-term variation features of haze days in Beijing and NCP. Quan et al. (2011) collected monitoring data and summarized the haze day occurrence trend over NCP for the past 56 years. These researchers also analyzed the effect of high aerosol loadings on haze formations by conducting a field measurement and found the important role of the hygroscopic growth of aerosols during the haze period. Yu et al. (2010) analyzed the aerosol optical properties during haze days in the past seven years and compared the features of single-scattering albedo and asymmetry factor during haze days with those during dust days in Beijing. This study also found that fine-mode particles were dominant in aerosol size distribution during haze days.

Numerous studies have used multiple methods to investigate the chemical and physical properties of

60 aerosols during haze occurrences in Beijing in different seasons. Li et al. (2013) identified the aerosol size
61 distribution and chemical composition from ground-based remote sensing measurements during haze
62 days in winter. Li et al. (2010) detected the aerosol components by using transmission electron
63 microscopy with energy-dispersive X-ray spectrometry during a haze episode in summer and determined
64 the influence of carbonaceous aerosols. Liu et al. (2013) and Zhao et al. (2013) conducted intensive field
65 experiments to identify the aerosol components of fine particles and discussed the constituent features of
66 $PM_{2.5}$ during the haze periods in autumn and winter, respectively. Wang et al. (2006) compared the
67 characteristics of aerosol components during dust, haze, and clean days. These previous works have
68 provided abundant information on the physical and chemical properties of aerosols during haze days.
69 However, the complex mechanism of haze formation over Beijing and its surrounding regions requires
70 further study. Various influencing factors, including meteorological field, key aerosol components, and
71 microphysical properties, should be comprehensively considered in investigating the relationship between
72 aerosols and surface visibility. Moreover, the seasonal similarities and differences of the haze formation
73 mechanism in Beijing remain unclear because most of these studies were generally focused on the
74 pollution periods in the same season.

75 In the present study, an air quality modeling system called Regional Atmospheric Modeling
76 System–Community Multi-scale Air Quality (RAMS–CMAQ) coupled with aerosol optical property
77 scheme is applied to simulate the meteorological field, the mass burden of major aerosol components
78 (sulfate, nitrate, ammonium, black carbon (BC), organic carbon (OC), dust, and sea salt), and the surface
79 visibility over NCP in 2011. The simulation results in February and July 2011 are selected and analyzed.
80 This study aims to discuss the contributions of various influencing factors to visibility deterioration and to
81 compare the differences of the haze formation mechanisms during winter and summer.

82

83 **2. Methodology**

84 The air quality modeling system RAMS–CMAQ was applied to concurrently simulate the
85 atmospheric and land processes that affect the transport, transformation, and deposition of aerosols and
86 their precursors. The major component of this modeling system is CMAQ (version 4.7), which was
87 developed by the US Environmental Protection Agency for assessing the effect of multiple pollutants,
88 including tropospheric ozone and other oxidants, aerosols, and acid deposition (Byun and Schere, 2006;
89 Eder and Yu, 2006; Eder et al., 2009; Mathur et al., 2008). The gas-phase chemistry mechanism was

90 updated to the expanded version CB05 (Sarwar et al., 2008). The thermodynamic equilibrium between
91 inorganic aerosol species and gas-phase concentrations was treated by ISORROPIA (Nenes et al., 1999).
92 Regional Particulate Model (Binkowski and Shankar, 1995) was used to describe the processes of aerosol
93 dynamics in CMAQ; such processes include new particle production, coagulation, and condensation
94 (Bhave et al., 2004; Yu et al., 2013). The formation of secondary organic aerosol (SOA) was mainly
95 treated by the CB05 mechanism, which was extended to allow for production of SOA from anthropogenic
96 and biogenic precursors. In the CB05, the SOA formation is modeled by forming semi-volatile products
97 in volatile organic compounds (VOCs) reactions. The semi-volatile products are partitioned between the
98 gas and aerosol phase according to the ambient conditions, such as temperature, relative humidity, vapor
99 pressure, existing aerosol particles. The aerosol particles in the modeling system were divided into three
100 modes, namely, Aitken, accumulation, and coarse modes (dust and sea salt). All modes were assumed to
101 follow the log normal distribution. The aerosol components, the geometric standard deviation, and the
102 geometric mean radius of each mode are listed in Table 1. The numerical prediction model RAMS was
103 coupled with CMAQ in the offline method to provide CMAQ with a meteorological field. A general
104 description of RAMS and its capabilities have been provided by Cotton et al. (2003). RAMS can describe
105 the boundary layer and the underlying surface effect, which is important for capturing air pollutants and
106 haze occurrence. The background meteorological fields and sea surface temperature were obtained from
107 the European Center for Medium-Range Weather Forecasts reanalysis datasets ($1^\circ \times 1^\circ$ spatial resolution)
108 and were based on weekly mean values and observed monthly snow cover information, respectively.

109 The anthropogenic emissions of precursors and primary aerosols (NO_x , SO_2 , VOCs, BC, OC, $\text{PM}_{2.5}$,
110 and PM_{10}) were obtained from the monthly-based emission inventory in China for 2010. This emission
111 inventory has a spatial resolution of $0.25^\circ \times 0.25^\circ$ and includes four categories, namely, power, industry,
112 residential, and transport (Lu et al., 2011). The nitrogen oxides and ammonia from soil were adopted from
113 the Global Emissions Inventory Activity $1^\circ \times 1^\circ$ monthly global inventory (Benkovitz et al., 1996). The
114 monthly mean inventory of Global Fire Emissions Database Version 2 (Randerson et al., 2007) was used
115 to provide the biomass burning emissions from forest wildfires, savanna burning, and slash-and-burn
116 agriculture. The online mechanisms introduced by Han et al. (2004) and Gong (2003) for capturing dust
117 and sea salt emissions, respectively, were included in the modeling system.

118 A scheme of aerosol optical properties was added to the modeling system to estimate the aerosol
119 extinction coefficient. This scheme contains a parameterization (Ghan and Zaveri, 2007) that efficiently

120 simplifies Mie theory calculation and maintains sufficient accuracy. Briefly speaking, the lognormal
121 distribution in each mode can be expressed as:

$$122 \quad \frac{dN}{d \ln D} = \frac{N}{(2\pi)^{1/2} \ln \sigma_g} \exp\left(-\frac{(\ln D - \ln D_p)^2}{2 \ln^2 \sigma_g}\right) \quad (1)$$

123 where N is the number concentration of aerosol particles, σ_g is the geometric standard deviation, D is the
124 particle diameter, and D_p is the geometric mean diameter. If refractive index and σ_g are given and the N is
125 set as a normalized value, the aerosol optical properties can be calculated by the Mie theory under several
126 size distributions with different D_p . The values of the specific optical properties under these size
127 distributions could be fitted by the Chebyshev polynomials with just five fitting coefficients.
128 Subsequently, the fitting coefficients table can be constructed with all possible values of refractive index
129 and σ_g . The scheme also applies Kohler theory (Pruppacher and Klett, 1997) and Maxwell–Garnett
130 mixing rule (Chuang et al., 2002) to describe the effects of water uptake and internal mixture, respectively.
131 The detailed description of this scheme can be found in Han et al. (2011). The visibility can be obtained
132 by using the following equation:

$$133 \quad VIS = 3.912/\beta \quad (2)$$

134 where VIS is the horizontal visibility, and β is the aerosol extinction coefficient (Seinfeld and Pandis,
135 1998). This modeling system simulated the mass concentration and optical properties of key aerosols in
136 previous studies on aerosol effects on the climate and environment in China (Han et al., 2013; Han et al.,
137 2011; Zhang et al., 2005, 2006, 2007).

138 For the simulation over NCP, a coarse domain that covers most of East Asia with a horizontal grid
139 distance of 64 km and a total area of 6654 km × 5440 km with a two-way nested inner domain was
140 established (Han et al., 2011). The inner domain (Fig. 1) has 94 × 90 grid cells and a 16 km resolution on
141 a rotated polar stereographic map projection centered at (116 °E, 40 °N). This domain includes all major
142 regions in NCP, namely, Beijing, Tianjin megacities and Hebei, Shandong, Shanxi provinces. Fifteen
143 vertical levels, nearly half of which were concentrated in the lowest 2 km, were used to improve the
144 simulation of the atmospheric boundary layer. The positions of the measurement stations applied for
145 model evaluation are marked on Fig. 1. The district areas of four major cities: Beijing, Tianjin,
146 Shijiazhuang, and Jinan were also shown in Fig. 1.

147

148 **3. Model evaluation**

149 In this section, the model simulations are compared with the observations. The meteorological driver
150 is an important factor in aerosol and visibility simulation. Wind vector, temperature, and relative humidity
151 are inherently related to aerosol transport, scavenging, and water uptake effect. Thus, the monitoring data
152 from the surface stations of the Chinese National Meteorological Center (CNMC;
153 (<http://cdc.cma.gov.cn/home.do>) were collected to evaluate the performance of the meteorological field
154 simulation. CNMC has 726 measurement stations that are evenly distributed throughout mainland China
155 and has been providing long-term surface observations of several meteorological variables since 1
156 January 1951 (Feng et al., 2004).

157 The comparative results of the daily average temperature, relative humidity, wind speed, and
158 maximum wind direction at eight stations in February and July are shown in Figs. 2 to 5, respectively.
159 The modeled temperature, relative humidity, and wind speed were in good agreement with the
160 observations at nearly all stations. A persistent underestimation of wind speed by the models was found at
161 the Wutaishan and Taishan sites. The modeled wind speed presented in Fig. 4 was obtained by converting
162 the output values of the first layer (90 m to 200 m) to near-surface wind (~10 m) according to
163 Monin–Obukhov similarity theory (Ding et al., 2001). These two sites are located on the mountainside at
164 elevations of 2208 and 1533 m, respectively. Thus, the underestimation may be attributed to the different
165 elevations between the simulation and the observation. As shown in Fig. 5, the modeled wind directions
166 did not coincide well with the observed data. A direct comparison is difficult to achieve because of the
167 difference in time resolutions between the site measurements (10 min, average) and the model output (1
168 h). Nevertheless, the variation trends of the modeled and observed wind directions are similar at most
169 sites, as shown in Fig. 5. The monthly modeled precipitation over NCP was compared to the observations
170 of surface monitoring data from 87 CNMC sites in Fig. 6. It can be seen that the modeling system
171 generally performed well on capturing the distribution patterns and seasonal variation features of
172 precipitation in Beijing, Tianjin megacities and Inner Mongolia, Hebei, Shandong provinces. However,
173 the modeled results underestimated the precipitation in North Beijing and north part of Hebei province in
174 July, which could cause the error of wet deposition estimation. The relative humidity was also
175 underestimated in the second half of February at Miyun and Tanggu sites and almost the whole July at
176 Miyun as shown in Fig. 3. Most of the underestimation generally happened when the relative humidity
177 exceeded 70%, which implied that the model was probably hard to capture the high water vapor over this
178 region. The comparison of modeled and observed precipitation and relative humidity in Beijing will be

179 discussed in detail below.

180 The modeled hourly NO₂, O₃, PM_{2.5}, and visibility in February and July were also compared with the
181 observed data provided by the Chinese Research Academy of Environmental Sciences (CRAES); CRAES
182 observes the real-time mass burden of air pollutants in Beijing (Gao et al., 2012). The comparative results
183 are shown in Figs. 7 and 9. The statistical parameters, including means, standard deviations, and
184 correlation coefficients between observation and simulation are listed in Table 2. These metrics can be
185 used to evaluate model performance (Yu et al., 2006). The model efficiently captured the daily variation
186 of the pollutant gases and the high mass burden of PM_{2.5} in these two months as shown in Fig. 7. Table 2
187 shows that most of the correlation coefficients are higher than 0.6, and the means and standard deviations
188 of simulations are also similar to those of observations. However, the correlation coefficients of PM_{2.5} and
189 NO₂ are lower than 0.5 in July. From Fig.7 and the means and standard deviations in Table 2, it can be
190 found that the model generally overestimated PM_{2.5} in the middle of July, and the fluctuation range of
191 modeled NO₂ was larger than that of the observation results. The comparison of modeled and observed
192 daily precipitation in Beijing is given in Fig. 8 (the observation data was collected from CNMC). It can be
193 seen that the modeled precipitation in July was obviously lower than that of observation in the middle of
194 July. This may result in weaker wet deposition which can cause overestimation of aerosol burden in
195 Beijing. For the simulated NO₂, the larger diurnal variation may be just caused by the uncertainties from
196 related gas-phase chemical scheme in CB05. The modeled visibility also agrees well with the
197 observations, particularly for visibility lower than 10 km, suggesting that the model can provide
198 reasonable simulation during haze occurrence. The means and standard deviations of modeled visibility
199 are quite similar to those of observations. Meanwhile, continuous haze can be found in the modeled and
200 observed results in the middle of July, as shown in Fig. 9. This phenomenon indicates that although the
201 model overestimated the mass burden of PM_{2.5}, the visibility simulation during this period remains
202 reliable. We also collected the hourly observation data of relative humidity from CRAES to evaluate the
203 model performance in Beijing, and the comparison is shown in Fig. 10. Even though the model
204 underestimated the relative humidity at Miyun and Tangshan sites, it can be found that the simulation
205 results followed the observed ones well in Beijing. The model just overestimated relative humidity when
206 its value was lower than about 30%. This evaluation indicates that the model could provide more
207 reasonable relative humidity in Beijing than that in Miyun and Tangshan.

208 The modeled daily average mass concentrations of major aerosol components were compared with

209 the observed data from the CRAES measurements, as shown in Fig. 11. The observed data lacked
210 information for the first half of February and a number of days in July because of instrument failure.
211 Although the magnitudes of the mass concentrations between the simulation and the observation do not
212 exactly agree with each other, the modeled results could broadly reproduce the peaks of the observed data
213 from February 20 to February 23 and from July 20 to July 23; the modeled results could also follow the
214 seasonal variation features. For instance, the modeled and observed carbonaceous aerosols were both high
215 in February and low in July. The model demonstrated obvious systematic underestimation of organic
216 carbon in these two months, as shown in Fig. 11. Numerous studies have reported that such phenomenon
217 is a common issue in regional chemistry and transport models (Heald et al., 2005; Koch et al., 2007). The
218 simulation error is primarily due to the uncertainties in the estimation of VOCs and primary organic
219 aerosol emissions and the formation mechanism of secondary organic aerosol (Kroll et al., 2006; Henze
220 and Seinfeld, 2006; Yu et al., 2007). However, this discrepancy should not significantly affect the
221 accuracy of the visibility simulation. Therefore, these evaluations suggest that the modeling system can
222 reasonably simulate the meteorological field, the mass burdens of major aerosol components, and the
223 surface visibility in February and July 2011.

224

225 **4. Results and discussions**

226 4.1 Distribution features of aerosol concentration and visibility

227 As shown in Figs. 7 to 11, two typical heavy air pollution episodes occurred over NCP from
228 February 20 to February 23 and from July 20 to July 23. These two periods were selected to investigate
229 the distribution features of pollutants and visibility over NCP during occurrences of heavy pollution in
230 different seasons. Fig. 12 presents the horizontal distributions of daily average mass concentration of
231 $PM_{2.5}$ and surface wind field over NCP from February 20 to February 23 and from July 20 to July 23. The
232 heavy mass burden of $PM_{2.5}$ (over $120 \mu g m^{-3}$) was mainly concentrated in Beijing and Tianjin megacities,
233 the whole area of Hebei province and northwest part of Shandong province. The mass concentration of
234 $PM_{2.5}$ in February, which exceeded $200 \mu g m^{-3}$ in Beijing, Tianjin, Shijiazhuang, and Jinan, was obviously
235 higher than that in July. The high mass burden of $PM_{2.5}$ appeared in the same regions as those in February
236 broadly ranged from $75 \mu g m^{-3}$ to $200 \mu g m^{-3}$ in July, and was rarely over $200 \mu g m^{-3}$ over the entire NCP.
237 The high mass burden of $PM_{2.5}$ in Beijing generally appeared when NCP was dominated by the south
238 wind field, which could have brought pollutants from the polluted regions in the south. The heavy $PM_{2.5}$

239 mass burden was also possibly transported to Northeast China and Bohai Sea by the strong south wind
240 from February 22 to February 23 and on July 23, respectively, thereby increasing the mass concentration
241 of $PM_{2.5}$ by $45 \mu\text{g m}^{-3}$ to $125 \mu\text{g m}^{-3}$ in these two regions, as shown in Fig. 12.

242 Fig. 12 also presents the horizontal distributions of daily average visibility and surface relative
243 humidity over NCP. The data shows that haze cloud could spread throughout NCP during each pollution
244 episode. The visibility in most parts of Hebei and Shandong was generally less than 8 km, which could
245 decrease to 3 km to 5 km in the four urban areas in February and July. The distribution patterns of
246 visibility broadly followed those of the $PM_{2.5}$ mass burden, and deteriorated visibility mainly appeared in
247 the regions where the heavy $PM_{2.5}$ mass burden is concentrated. The visibility generally decreased to 3
248 km to 5 km when the mass concentration of $PM_{2.5}$ exceeded $200 \mu\text{g m}^{-3}$ in February. However, similar
249 values of visibility also appeared in July when the mass concentration of $PM_{2.5}$ was merely in the range of
250 $120 \mu\text{g m}^{-3}$ to $200 \mu\text{g m}^{-3}$. Such phenomenon was demonstrated on July 23 when the visibility over the
251 entire Bohai Sea generally ranged from 3 km to 5 km and the mass concentration of $PM_{2.5}$ was
252 maintained between 120 and $200 \mu\text{g m}^{-3}$. These differences may be due to the strong extinction of soluble
253 particles caused by the high relative humidity (exceeding 70%) in July, as shown in Fig. 12. This feature
254 is discussed in detail below.

255 4.2 Meteorological factors, major aerosol components and their contributions to extinction in Beijing

256 Figs. 13(a) to 13(h) present the time series of regional average surface wind speed, and relative
257 humidity, visibility, as well as the mass concentrations of $PM_{2.5}$, sulfate, nitrate, ammonium, BC, and OC
258 in Beijing in February and July 2011. The averages of these variables during the haze days in February
259 and July are shown in Table 3. The mass burden of $PM_{2.5}$ is the most important influencing factor of
260 visibility change because it is generally inversely correlated with the variation of visibility. The mass
261 concentrations of three kinds of inorganic salt, namely, nitrate, sulfate, and ammonium, suggest that they
262 were the three major aerosol components of $PM_{2.5}$ in Beijing, as shown in Figs. 13(e) to 13(f). **The mass
263 burden of organic carbon was comparable with that of nitrate, which means that the total mass burden of
264 organic matter should be larger than that of nitrate. If not consider the total organic matter, nitrate should
265 be the main particulate pollutant during winter because the mass burden of nitrate was obviously higher
266 than those of the other components in February.** Although the diurnal variation of nitrate concentration
267 was significant in July, the daily maximum nitrate concentration was still larger than that of sulfate
268 concentration during nighttime. These findings suggest that the emission from the transportation sector is

269 currently the major source of secondary particles in Beijing. The mass burden of carbonaceous aerosols
270 was high in February and low in July. In addition to the diffusion conditions, the strong emissions of coal
271 and biomass burning are the main reasons for the high values of carbonaceous aerosols during winter
272 (Zhang et al., 2014).

273 As shown in Table 3, July had a greater number of haze days than February, and the average
274 visibility during haze days in July was lower than that in February. These features indicate that air
275 pollution was more serious in July than in February. However, the average mass concentration of PM_{2.5} in
276 July during haze days was obviously lower than that in February. In addition, Table 3 shows that the
277 relatively low value of PM_{2.5} mass concentration in July was primarily due to the small quantities of
278 carbonaceous aerosol burden. Meanwhile, the total mass burden of nitrate, sulfate, and ammonium was
279 higher in July than in February. Therefore, the deteriorated visibility is caused by the simultaneous
280 occurrence of high mass burden of soluble particles and high relative humidity in July. The difference in
281 the haze formation mechanism during winter and summer should be associated with the different
282 constructions of PM_{2.5} components and the ambient relative humidity.

283 Fig. 13(g) to 13(h) present the time series of the regional average contribution ratios of sulfate,
284 nitrate, ammonium, BC, OC, and other components (dust, sea salt, and unspecified anthropogenic mass)
285 to the total surface extinction in Beijing in February and July. The monthly mean of these contribution
286 ratios are shown in Table 4. The contribution ratios were calculated by subtracting the extinction
287 coefficient with and without each aerosol component when estimated the aerosol optical properties by
288 using the scheme introduced in section 2. Nitrate, sulfate, and ammonium, which are inorganic salts,
289 significantly contributed to the surface extinction in Beijing, which was ~70% in February and over 80%
290 in July. Carbonaceous aerosol provided nearly 20% and 5% contribution in February and July,
291 respectively, whereas other aerosol components provided ~10% contribution. These ratios generally
292 followed the magnitude of their mass concentrations. Except for the diurnal variation of nitrate in July,
293 the contribution ratios of each aerosol component did not significantly change when the mass
294 concentration of PM_{2.5} exceeded ~50 μg m⁻³. By contrast, when the mass concentration of PM_{2.5}
295 decreased to less than 50 μg m⁻³, the contribution ratios of carbonaceous aerosol and other components
296 obviously increased. A higher mass concentration of PM_{2.5} corresponds to higher contribution ratios of
297 the three inorganic salts. This feature confirms that nitrate, sulfate, and ammonium are the major aerosol
298 components that influence the haze formation in Beijing.

299 4.3 Haze occurrence threshold in Beijing

300 It can be seen from Fig. 13 that the mass concentration of $PM_{2.5}$ was closely inversely correlated
301 with visibility. However, when the mass concentration of $PM_{2.5}$ located in different value intervals, the
302 influence on the visibility was not consistent. Fig. 14(a) shows the time series of regional mean mass
303 concentration of $PM_{2.5}$ and visibility in Beijing from 23 to 25 July. As is seen, the air qualities in these
304 three days turned to good and the visibility continuously increased. The mass concentration of $PM_{2.5}$
305 decreased from $260 \mu g m^{-3}$ on 23 July to $20 \mu g m^{-3}$ on 25 July. For the convenience of distinguishing, the
306 decreasing process is divided into **period A**, B and C in the figure. Then, it can be found that in **period A**,
307 the mass concentration of $PM_{2.5}$ changed from $260 \mu g m^{-3}$ to $120 \mu g m^{-3}$, decreasing by about $140 \mu g m^{-3}$
308 while the visibility increased by less than 5 km; in **period B**, the mass concentration of $PM_{2.5}$ changed
309 from $120 \mu g m^{-3}$ to $50 \mu g m^{-3}$, decreasing by about $70 \mu g m^{-3}$ and the visibility increased obviously, from
310 5km to about 20 km; finally, in **period C**, the mass concentration of $PM_{2.5}$ changed from $35 \mu g m^{-3}$ to 20
311 $\mu g m^{-3}$, decreasing by only $15 \mu g m^{-3}$ and the visibility increased dramatically by 60 km. The above
312 analysis indicated that even though the emission reduction measures are taken to dramatically decrease
313 the $PM_{2.5}$ mass burden, the improvement of visibility would still be weak if the mass concentration of
314 $PM_{2.5}$ keeps in a high level. Only when the mass concentration of $PM_{2.5}$ is decreased to the certain value
315 range can the visibility be improved greatly and it is easier for the visibility to be over 10 km. **The**
316 **visibility was calculated by using the formula (2) in the modeling system. Thus, the aerosol extinction**
317 **coefficient should be the key factor influencing the visibility. From Fig. 14(b), it can be seen that the**
318 **variation of extinction coefficient and mass concentration of $PM_{2.5}$ were quite similar with each other. We**
319 **can deduce that when the value of extinction coefficient becomes small, the value of visibility could**
320 **change dramatically with a microvariation of extinction coefficient by using formula (2). This should be**
321 **the main reason of the drastic change of visibility during period C.** Therefore, strictly speaking it is
322 necessary to distinguish the atmospheric haze and the atmospheric pollution. The improvement of
323 atmospheric quality (mass concentrations of pollutants decrease) does not mean the haze disappears. If
324 the occurrence of haze is controlled by decreasing mass concentration of $PM_{2.5}$ in atmosphere, it is more
325 reasonably to set a haze occurrence threshold interval (the values of mass concentration of $PM_{2.5}$ when
326 the visibility reaches 10 km in different ambient conditions). Only by strictly keeping the mass
327 concentration of $PM_{2.5}$ below this threshold can the visibility be effectively improved. Otherwise, even
328 though the emission reduction measures are taken when heavy pollution event appears, the improvement

329 of visibility would still be very weak if the mass concentration of PM_{2.5} fails to fall into the values of haze
330 occurrence threshold. Furthermore, the specific value of the threshold should be closely related to the
331 pollutant characteristics, meteorological conditions and other factors.

332 A sensitivity test was conducted to evaluate the mass concentration threshold of PM_{2.5} to cause haze
333 occurrence in Beijing. First, the mass ratio of each aerosol component to the total mass burden of all
334 aerosol particles was calculated from the results of the model simulation at every grid point. Then, the
335 sensitivity run was conducted by using several possible values of the total aerosol burden and following
336 the same ratio of each aerosol component at the same grid points to identify the mass concentration
337 threshold of PM_{2.5} when the visibility decreased to 10 km under different relative humidity. The values of
338 relative humidity were chosen as follows: 70%, 75%, 80%, 85%, 88%, 89%, and 90%. Lower values of
339 relative humidity were disregarded because the water uptake of soluble particles is insignificant when the
340 relative humidity is less than 70%. **The value of relative humidity higher than 90% indicate that the light**
341 **fog occurred as expressed by Wu et al. (2007).** Figs. 15(a) and 15(b) present the time series of the
342 regional average threshold of haze occurrence under different values of relative humidity from the
343 sensitivity test in February and July in Beijing. The threshold changed significantly with the variation in
344 relative humidity, and its declining trend increased with increasing relative humidity. The range of mass
345 concentration threshold reached 30 $\mu\text{g m}^{-3}$ when the relative humidity changed from 70% to 90%.
346 Conversely, the threshold generally maintained a small **change** ($<5 \mu\text{g m}^{-3}$) when the relative humidity
347 was fixed. This indicated that if the aerosol components do not have dramatic variation in Beijing, a
348 relatively fixed haze occurrence threshold could be determined.

349 However, the mass concentration threshold on July 29 could increase by approximately 10 $\mu\text{g m}^{-3}$
350 under the same relative humidity, as shown in Fig. 15(b). Further analysis showed that this phenomenon
351 might be related to the variation of aerosol in accumulation mode. Figs. 15(c) to 15(h) present the time
352 series of the regional average mass ratios and contribution ratios of the three particle modes to the total
353 aerosol burden and the total extinction, respectively. As is seen from Fig. 15(e) and 15(h), the extinction
354 contribution of accumulation mode particles was above 97% due to the high mass concentration ratio and
355 extinction efficiency. However, it can be found that the extinction contribution of accumulation mode
356 particles on 29 July obviously decreased by about 5%. Therefore, it can be deduced there should be a high
357 correlation between the haze occurrence threshold and extinction contribution of accumulation mode
358 particles. Furthermore, it can be seen from Fig. 15(j) that the visibility on 29 July rose from less than 5km

359 to more than 20km rapidly. Thus, it can be deduced that a weather process which was beneficial to the
360 pollutant scavenging eliminated the mass concentration of accumulation mode particles efficiently (the
361 new particles in the atmosphere could be eliminated immediately before coagulation or condensation) in
362 this period. Then, the mass concentration ratio and extinction contribution ratio of Aitken mode particles
363 could be increased about 10% and 5%, respectively. These should be the major reason for the decreasing
364 extinction contribution ratio of accumulation mode particles. The similar weather processes also occurred
365 on 2-3, 5-10, and 25 July. It can be found that during these periods the mass concentration of
366 accumulation mode particles decreased significantly. However, different from the condition on 29 July,
367 the mass concentration ratio and extinction contribution of Aitken mode particles did not change
368 obviously, but the mass concentration ratio of coarse mode particles increased dramatically in these three
369 processes. It is found that though the mass concentration of coarse mode particles accounted for 10%-20%
370 of the total aerosol, its extinction contribution was only below 1% in most periods. Therefore, except
371 some special cases (e. g., dust event), the influence of coarse mode particles on extinction should be
372 obviously weaker than other modes. This was also the main reason for no significant variation of
373 extinction contribution ratio of accumulation mode particles in these three processes.

374 Generally speaking, besides relative humidity, haze occurrence threshold is also sensitive to the
375 extinction contribution ratio of accumulation mode particles. Seen from the above analysis, the mass
376 concentration ratio of accumulation mode particles generally remained at high level and the fluctuation
377 range was small during the heavy pollution episode in Beijing, which can ensure the variation range of
378 haze occurrence threshold was less than $5 \mu\text{g m}^{-3}$ when the relative humidity was fixed. The increase of
379 haze occurrence threshold due to the variation of extinction contribution of accumulation mode particles
380 only appeared when the mass burden of Aitken mode particles increased in clean period. The reason for
381 this phenomenon should be that the extinction efficiency of Aitken mode particles is far smaller than that
382 of accumulation mode particles. Therefore, more Aitken mode particles are needed to form the haze.
383 However, the smaller particles generally exist during the clean period as shown by the simulation results,
384 which means the haze does not appear. Thus, the influence of extinction contribution of accumulation
385 mode particles on haze occurrence threshold can be neglected in Beijing in most cases. The relative
386 humidity should be the only impact factor which needs to be considered.

387 The monthly means of the threshold of haze occurrence are shown in Table 5. It can be seen from
388 Table 5 that when the relative humidity changed from 70% to 90%, the threshold interval increased from

389 52 $\mu\text{g m}^{-3}$ to 83 $\mu\text{g m}^{-3}$. In a certain relative humidity, the average monthly thresholds were similar in
390 February and July. Here, the relationship between haze occurrence threshold and relative humidity was
391 fitted by the exponential function, and below is the formula:

$$392 \quad RH = a + b \times \exp(c \times M) \quad (2)$$

393 where RH represents relative humidity; M represents the $\text{PM}_{2.5}$ mass concentration threshold; a , b and c
394 represent fitting parameters, and their values are listed in Table 6. The fitting curve is shown in Fig. 16.
395 From Table 6 it can be seen that the values of R^2 are all higher than 0.9, which indicates that their
396 relationship can be described by exponential function well. Therefore, the fitting curves given in Fig. 16
397 can be used to capture the haze occurrence threshold in Beijing. In a certain relative humidity (not higher
398 than 90% as the definition of haze), when $\text{PM}_{2.5}$ mass concentration increases beyond the corresponding
399 values on the curve, the haze should be easy to appear. Furthermore, the analysis in this study also
400 indicated that the haze occurrence can be efficiently controlled by strictly restricting the $\text{PM}_{2.5}$ mass
401 concentration near or below the fitting curve. Otherwise, the great decrease of $\text{PM}_{2.5}$ mass burden would
402 not obviously reduce the possibility of haze occurrence.

403

404 5. Conclusions

405 In this study, the air quality modeling system RAMS-CMAQ coupled with an aerosol optical
406 property scheme was used to simulate the meteorological field, the mass concentration of aerosols, and
407 the surface visibility over NCP in 2011. The modeling system provided reliable simulation results. The
408 distribution patterns and time series of related meteorological factors and aerosol characteristic in
409 February and July 2011 were analyzed to elucidate the seasonal variation features of the haze formation
410 mechanism in Beijing and its surrounding regions. In addition, a sensitivity test was conducted to
411 investigate the $\text{PM}_{2.5}$ mass concentration threshold of haze occurrence in Beijing under distinct conditions.
412 The results are summarized as follows:

413 (1) The simulation results showed that the high mass burden of $\text{PM}_{2.5}$ over NCP was mainly
414 concentrated in Beijing and Tianjin megacities, the whole area of Hebei province and northwest part of
415 Shandong province. The daily average mass concentration of $\text{PM}_{2.5}$ over these regions was generally over
416 120 $\mu\text{g m}^{-3}$ during the pollution episodes in February and July. The worst air quality over NCP was found
417 in Beijing because of the heavy daily average mass burden of $\text{PM}_{2.5}$, which exceeded 300 $\mu\text{g m}^{-3}$ in
418 February. The south wind that carries pollutants from the southern regions is an important source of the

419 heavy aerosol loading in Beijing. In addition to the horizontal diffusion, the vertical convection also plays
420 an important role in the pollutant scavenging in Beijing.

421 (2) The distribution patterns of visibility generally followed those of the $PM_{2.5}$ mass burden. The
422 daily average visibility below 10 km covered most regions of NCP during the pollution episodes in
423 February and July and was below 5 km over the urban areas. The daily average relative humidity rarely
424 exceeded 90%, suggesting that the haze cloud could spread throughout NCP when the pollution episode
425 appears in both winter and summer.

426 (3) The simulation results showed that nitrate, sulfate, and ammonium were the three major aerosol
427 components and the main causes of the visibility deterioration in Beijing. The mass burdens of these three
428 inorganic salts were obviously higher than those of other aerosols, and their total contribution ratios to
429 surface extinction reached 70% in February and 85% in July. Nitrate was also the first and second major
430 contributor to surface extinction in February and July, respectively, implying that the emission from the
431 transportation sector is currently the major source of secondary particles in Beijing. The carbonaceous
432 aerosols accounted for 15% extinction in February and below 5% extinction in July. This feature indicates
433 that the pollution status and emission sources were more complicated during winter in Beijing.

434 (4) The haze formation mechanism in Beijing in winter is obviously different from that in summer.
435 Firstly, the mass concentration of $PM_{2.5}$ in winter was relatively higher and the components were
436 complicated. The ratios of inorganic salts and carbonaceous aerosols were generally balanced. Therefore,
437 the high mass concentration of $PM_{2.5}$ and diverse aerosol components should be the major reasons of the
438 serious haze occurrence in winter. While the mass concentration of $PM_{2.5}$ in summer was relatively lower
439 than that in winter, but the ratio of hygroscopic inorganic salts, including sulfate, nitrate and ammonium,
440 increased and their mass concentrations were even higher than those in winter. With obviously higher
441 relative humidity, it could still form serious haze with equal level to winter even the mass concentration
442 of $PM_{2.5}$ is lower than that in winter. The water uptake of hygroscopic components played a key role in it.
443 This indicated that it is important to apply emission reduction measures based on the specific pollution
444 and meteorological characteristics in different seasons. In this way, the possibility of haze occurrence can
445 be effectively decreased.

446 (5) From analysis, it can be found that even though the mass concentration of $PM_{2.5}$ is closely
447 inversely correlated with visibility, the influence effect is diversity when the mass concentration of $PM_{2.5}$
448 locates in different intervals. When the mass concentration of $PM_{2.5}$ is relatively high (larger than $100 \mu g$

449 m^{-3}), the influence of its variation on visibility is very weak. Only when the mass concentration of $\text{PM}_{2.5}$
450 is cut down to a certain interval can its decrease make the visibility increase rapidly. Therefore, it is more
451 reasonably to set a haze occurrence threshold interval (the values of mass concentration of $\text{PM}_{2.5}$ when
452 the visibility reaches 10 km in different ambient conditions). If the mass concentration of $\text{PM}_{2.5}$ fails to
453 fall into the values of haze occurrence threshold, the improvement of visibility would still be very weak
454 when the emission reduction measures are taken.

455 (6) Through the sensitivity experiment, this study estimated the haze occurrence threshold interval in
456 Beijing, and discussed related impact factors. Generally speaking, if the components of $\text{PM}_{2.5}$ do not have
457 dramatic variation in Beijing, the haze occurrence threshold is just sensitive to the extinction contribution
458 ratio of accumulation mode particles and relative humidity. In consideration of the variation of extinction
459 contribution ratio of accumulation mode particles generally occurs in the clean period, the relative
460 humidity should be the only impact factor which needs to be considered. Finally, the relationship between
461 threshold of haze occurrence and relative humidity in winter and summer in Beijing was fitted by the
462 exponential function, and these fitting curves could be a new theoretical basis for the further
463 understanding and control of the haze formation in Beijing. **As analysis in this study, the fitting function
464 could be applied to diagnose the haze happen under ordinary situation in Beijing. However, this function
465 should not be suitable for the haze happened over other region or uncommon pollution episodes (e.g. the
466 dust storm) occur in Beijing because the ratio of major aerosol components and particle size distribution
467 would be different. The further study is still necessary for other regions and various pollution features.**

468
469
470
471
472
473
474
475
476
477

Reference

- 478
- 479 Benkovitz, C., Schultz, M., Pacyna, J., Tarrason, L., Dignon, J., Voldner, E., Spiro, P., Logan, J., and
480 Graedel, T.: Global gridded inventories of anthropogenic emissions of sulfur and nitrogen, *J.*
481 *Geophys. Res.*, 101, 29239-29254, 1996.
- 482 Bhave, P. V., Roselle, S. J., Binkowski, F. S., Nolte, C. G., Yu, S. C., Gipson, G. L., and Schere, K. L.:
483 CMAQ Aerosol Module Development: Recent Enhancements and Future Plans, Paper presented at
484 3rd Annual CMAS Models-3 Users' Conference, Commun. Model., and Anal. Syst. Cent., Chapel
485 Hill, N.C., 18-20 October, 2004.
- 486 Binkowski, F. S. and Shankar, U.: The regional particulate model, 1, Model description and preliminary
487 results, *J. Geophys. Res.*, 100, 26191-26209, 1995.
- 488 Byun, D. and Schere, K.: Review of the governing equations, computation algorithms, and other
489 components of the Models-3 Community Multiscale Air Quality (CMAQ) modeling system. *Appl.*
490 *Mech. Rev.*, 59, 51-77, 2006.
- 491 Chuang, C., Penner, J., Prospero, J., Grant, K., Rau, G., and Kawamoto, K.: Cloud susceptibility and the
492 first aerosol indirect forcing: sensitivity to black carbon and aerosol concentrations, *J. Geophys. Res.*,
493 107, doi: 10.1029/2000JD000215, 2002.
- 494 Cotton, W., Pielke, R., Walko, G., Liston, G., Tremback, C., Jiang, H., McAnelly, R., Harrington, J.,
495 Nicholls, M., Carrio, G., and McFadden, J.: RAMS 2001: current status and future directions,
496 *Meteorol. Atmos. Phys.*, 82, 5-29, 2003.
- 497 Ding, F., Pal Arya, S., and Lin, Y.: Large-eddy simulations of the atmospheric boundary layer using a new
498 subgrid-scale model-II. Weakly and moderately stable cases, *Environ. Fluid Mech.*, 1, 49-69, 2001.
- 499 Eder, B., Kang, D., Mathur, R., Pleim, J., Yu, S. C., Otte, T., and Pouliot, G.: A performance evaluation of
500 the national air quality forecast capability for the summer of 2007, *Atmos. Environ.*, 43, 2312-2320,
501 2009.
- 502 Eder, B. and Yu, S. C.: An evaluation of model performance of EPA models-3/CMAQ, *Atmos. Environ.*,
503 40, 4811-4824, 2006.
- 504 Feng, S., Hu, Q., and Qian, W.: Quality control of daily meteorological data in China, 1951-2000: a new
505 dataset. *Int. J. Climatol.*, 24, 853-870, 2012.
- 506 Gao, J., Zhang, Y., Wang, S., Chi, F., and Chen, Y.: Study on the Characteristics and Formation of a
507 Multi-Day Haze in October 2011 in Beijing, *Res. Environ. Sci. (in Chinese)*, 25, 1201-1207, 2012.
- 508 Ghan, S., and Zaveri, R.: Parameterization of optical properties for hydrated internally mixed aerosol, *J.*
509 *Geophys. Res.*, 112, D10201, doi:10.1029/2006JD007927, 2007.
- 510 Gong, S. L.: A parameterization of sea-salt aerosol source function for sub- and super-micron particles,
511 *Global Biogeochem. Cy.*, 17, doi: 10.1029/2003GB002079, 2003.
- 512 Han, X., Zhang, M., Han, Z., Xin, J., and Liu, X.: Simulation of aerosol direct radiative forcing with
513 RAMS-CMAQ in East Asia, *Atmos. Environ.*, 45, 6576-6592, 2011.
- 514 Han, X., Zhang, M., Tao, J., Wang, L., Gao, J., Wang, S., Chai, F.: Modeling aerosol impacts on
515 atmospheric visibility in Beijing with RAMS-CMAQ, *Atmos. Environ.*, 72, 177-191, 2013.
- 516 Han, Z., Ueda, H., Matsuda, K., Zhang, R., Arao, K., Kanai, Y., and Hasome, H.: Model study on particle
517 size segregation and deposition during Asian dust events in March 2002, *J. Geophys. Res.*, 109, doi:
518 10.1029/2004JD004920, 2004.
- 519 Hao, J. and Wang, L.: Improving Urban Air Quality in China: Beijing Case Study, *Air Waste Manage.*
520 *Assoc.*, 62, 1298-1305, 2012.

521 Heald, C. L., Jacob, D. J., Park, R. J., Russell, L. M., Huebert, B. J., Seinfeld, J. H., Liao, H., and Weber,
522 R. J.: A large organic aerosol source in the free troposphere missing from current models, *Geophys.*
523 *Res. Lett.*, 32, L18809, doi:10.1029/2005GL023831.

524 Henze, D. K. and Seinfeld, J.H.: Global secondary organic aerosol from isoprene oxidation, *Geophys. Res.*
525 *Lett*, 33:L09812, doi:10.1029/2006GL025976, 2006.

526 Koch, D., Bond, T. C., Streets, D., Unger, N., van der Werf, G. R.: Global impact of aerosols from
527 particular source regions and sectors, *J. Geophys. Res.*, 112, D02205, doi:10.1029/2005JD007024,
528 2007.

529 Kroll, J. H., Ng, N. L., Murphy, S. M., Flagan, R. C., and Seinfeld, J. H.: Secondary organic aerosol
530 formation from isoprene photooxidation, *Environ. Sci. Technol.*, 40, 1869-1877, 2006.

531 Li, W., Shao, L., Buseck, P.: Haze types in Beijing and the influence of agricultural biomass burning,
532 *Atmos. Chem. Phys.*, 10, 8119-8130, 2010.

533 Li, Z., Gu, X., Wang, L., Li, D., Li, K., Dubovik, O., Schuster, G., Goloub, P., Zhang, Y., Li, L., Xie, Y.,
534 Ma, Y., and Xu, H.: Aerosol physical and chemical properties retrieved from ground-based remote
535 sensing measurements during heavy haze days in Beijing winter, *Atmos. Chem. Phys.*, 13,
536 5091-5122, 2013.

537 Liu, X., Li, J., Qu, Y., Han, T., Hou, L., Gu, J., Chen, C., Yang, Y., Liu, X., Yang, T., Zhang, Y., Tian, H.,
538 and Hu, M.: Formation and evolution mechanism of regional haze: a case study in the megacity
539 Beijing, China, *Atmos. Chem. Phys. Discuss.*, 12, 16259-16292, 2012.

540 Lu, Z., Streets, D. G., Zhang, Q., Wang, S., Carmichael, G. R., Cheng, Y. F., Wei, C., Chin, M., Diehl, T.,
541 and Tan, Q.: Sulfur dioxide emissions in China and sulfur trends in East Asia since 2000, *Atmos.*
542 *Chem. Phys.*, 10, 6311–6331, 2010.

543 Lu, Z, Zhang, Q, Streets, D.: Sulfur dioxide and primary carbonaceous aerosol emissions in China and
544 India, 1996–2010. *Atmospheric Chemistry and Physics*, 11: 9839-9864, 2011.

545 Ma, J., Xu, X., Zhao, C., Yan, P.: A review of atmospheric chemistry research in China: Photochemical
546 smog, haze pollution, and gas-aerosol interactions. *Adv. Atmos. Sci.*, 29, 1006-1026, 2010.

547 Mathur, R., Yu, S. C., Kang, D., and Schere, K. L.: Assessment of the winter-time performance of
548 developmental particulate matter forecasts with the Eta-CMAQ modeling system, *J. Geophys. Res.*,
549 113, D02303, doi:10.1029/2007JD008580, 2008.

550 Nenes, A., Pandis, S., and Pilinis, C.: Continued development and testing of a new thermodynamic
551 aerosol module for urban and regional air quality models, *Atmos. Environ.*, 33, 1553-1560, 1999.

552 Pruppacher, H. and Klett, J.: *Microphysics of Clouds and Precipitation*. Springer, New York. p. 954, 1997.

553 Quan, J., Zhang, Q., He, H., Liu, J., Huang, M., and Jin, H.: Analysis of the formation of fog and haze in
554 North China Plain (NCP), *Atmos. Chem. Phys.*, 11, 8214-8250, 2011.

555 Randerson, J. T., van der Werf, G. R., Giglio, L., Collatz, G. J., and Kasibhatla, P. S.: Global Fire
556 Emissions Database, Version 2 (GFEDv2.1), Data set available on-line (<http://daac.ornl.gov/>) from
557 Oak Ridge National Laboratory Distributed Active Archive Center, Oak Ridge, Tennessee, USA,
558 doi:10.3334/ORNLDAAAC/849, 2007.

559 Sarwar, G., Luecken, D., Yarwood, G., Whitten, G., and Carter, W.: Impact of an updated carbon bond
560 mechanism on predictions from the CMAQ modeling system: preliminary assessment, *J. Appl.*
561 *Meteorol. Clim.*, 47, 3-14, 2008.

562 Seinfeld, J. and Pandis, S.: *Atmospheric Chemistry and Physics*. Wiley, New York, USA, 1998.

563 Sun, Y., Zhuang, G., Tang, A., Wang, Y., and An, Z.: Chemical characteristics of PM_{2.5} and PM₁₀ in
564 Haze-Fog episodes in Beijing, *Environ. Sci. Technol.*, 40, 3148-3155, 2006.

565 Tao, M., Chen, L., Su, L., and Tao, J.: Satellite observation of regional haze pollution over the North
566 China Plain, *J. Geophys. Res.*, 117, D12203, DOI: 10.1029/2012JD017915, 2012.

567 Wang, X., Sun, M., Yang, T., and Wang, Z.: Interdecadal change in frequency of dust-haze episodes in
568 North China Plain, *Clim. Environ. Res.* (in Chinese), 18, 165-170, 2013.

569 Wang, Y., Zhuang, G., Sun, Y., An, Z.: The variation of characteristics and formation mechanisms of
570 aerosols in dust, haze, and clear days in Beijing, *Atmos. Environ.*, 40, 6579-6591, 2006.

571 Wu, D., Bi, X., Deng, X., Li, F., Tan, H.: Effect of atmospheric haze on the deterioration of visibility over
572 the Pearl River Delta, *Acta Geogr. Sin.* (in Chinese), 21, 215-223, 2007.

573 Yu, S. C., Bhave, P. V., Dennis, R. L., and Mathur, R.: Seasonal and regional variations of primary and
574 secondary organic aerosols over the continental United States: semi-empirical estimates and model
575 evaluation, *Environ. Sci. Technol.*, 41, 4690-4697, 2007.

576 Yu, S. C., Eder, B., Dennis, R., Chu, S. H., and Schwartz, S.: New unbiased symmetric metrics for
577 evaluation of air quality models, *Atmos. Sci. Lett.*, 7, 26-34, 2006.

578 Yu, S. C., Mathur, R., Pleim, J., Wong, D., Gilliam, R., Alapaty, K., Zhao, C., and Liu, X.: Aerosol
579 indirect effect on the grid-scale clouds in the two-way coupled WRF-CMAQ: model description,
580 development, evaluation and regional analysis, *Atmos. Chem. Phys. Discuss.*, 13, 25649-25739,
581 2013.

582 Yu X, Zhu B, Yin Y, Yang J, Li Y, and Bu, X.: A comparative analysis of aerosol properties in dust and
583 haze-fog days in a Chinese urban region. *Atmos. Res.*, 99, 241-247, 2011.

584 Zhang, A., Qi, Q., Jiang, L., Zhou, F., and Wang, J.: Population exposure to PM_{2.5} in the urban area of
585 Beijing, *PloS one*, 8, e63486, 2013.

586 Zhang, J., Miao, H., Ouyang, Z., and Wang, X.: Ambient air quality trends and driving factor analysis
587 since 1980's in Beijing, *Acta Sci. Circumstantiae* (in Chinese), 26, 1886-1892, 2006.

588 **Zhang, J., Sun, Y., Liu, Z., Ji, D., Hu, B., Liu, Q., and Wang, Y.: Characterization of submicron aerosols**
589 **during a month of serious pollution in Beijing, 2013, *Atmos. Chem. Phys.*, 14, 2887-2903, 2014.**

590 Zhang, J., Zhu, T., Zhang, Q., Li, C., Shu, H., Ying, Y., Dai, Z., Liu, X., Liang, A., and Shen, H.: The
591 impact of circulation patterns on regional transport pathways and air quality over Beijing and its
592 surroundings, *Atmos. Chem. Phys.*, 11, 5031-5053, 2012.

593 Zhang, M., Gao, L., Ge, C., and Y.: Simulation of nitrate aerosol concentrations over East Asia with the
594 model system RAMS-CMAQ, *Tellus B*, 59, 372-380, 2007.

595 Zhang, M., Xu, Y., Zhang, R., and Han, Z.: Emission and concentration distribution of black carbon
596 aerosol in East Asia during springtime, *Chin. J. Geophys.*, 48, 55-61, 2005.

597 Zhang, M., Uno, I., Zhang, R., Han, Z., Wang, Z., and Pu, Y.: Evaluation of the Models-3 Community
598 Multi-scale Air Quality (CMAQ) modeling system with observations obtained during the TRACE-P
599 experiment: comparison of ozone and its related species, *Atmos. Environ.*, 40, 4874-4882, 2006.

600 Zhao, P., Zhang, X., Xu, X., and Zhao, X.: Long-term visibility trends and characteristics in the region of
601 Beijing, Tianjin, and Hebei, China, *Atmos. Res.*, 101, 711-718, 2011.

602 Zhao, X., Zhao, P., Xu, J., Meng, W., Pu, W., Dong, F., He, D., and Shi, Q.: Analysis of a winter regional
603 haze event and its formation mechanism in the North China Plain, *Atmos. Chem. Phys.*, 13,
604 5685-5696, 2013.

605
606
607

608

Table 1 Aerosol size distribution parameters in RAMS-CMAQ.

Mode	Aerosol components	σ^a	r^b , μm
Aitken	ASO ₄ ^c , ANO ₃ ^d , ANH ₄ ^e , BC ^f , OC ^g	1.7	0.015
Accumulation	ASO ₄ , ANO ₃ , ANH ₄ , BC, OC, Dust, Sea salt	2.0	0.150
Coarse dust	Dust	3.0	0.300
Coarse sea salt	Sea salt	3.5	0.300

609 ^a σ is geoetric standard deviation.610 ^b r is mode radius.611 ^c ASO₄ represents sulfate aerosol.612 ^d ANO₃ represents nitrate aerosol.613 ^e ANH₄ represents ammonium aerosol.614 ^f BC represents black carbon.615 ^g OC represents organic carbon.

616

617

618

619

620

621

622

623

624

625

626

627

628

629

630

631

632

633

634

635

636

637

638

639

640

641

642

643

644

645

646

647
648

649
650
651
652
653
654
655
656
657
658
659
660
661
662
663
664
665
666
667
668
669
670
671
672
673
674
675
676
677
678
679
680
681

Table 2 Statistic summary of the comparisons of PM_{2.5}, O₃, NO₂, and visibility between simulation and observation in Beijing

		N^a	C_{mod}^b	C_{obs}^c	σ_{mod}^d	σ_{obs}^e	R^f
PM _{2.5}	Feb	665	133.05	127.5	102.41	129.7	0.76
	Jul	663	112.78	89.92	74.09	72.98	0.43
O ₃	Feb	621	15.74	16.10	14.04	14.04	0.78
	Jul	630	56.59	48.75	38.44	36.21	0.74
NO ₂	Feb	672	33.94	44.18	17.59	24.98	0.75
	Jul	626	25.29	24.08	17.01	11.62	0.42
Visibility	Feb	672	10.97	10.78	6.53	7.27	0.76
	Jul	744	8.06	9.64	5.74	6.48	0.65

^aNumber of samples.
^bTotal mean of observations.
^cTotal mean of simulations.
^dStandard deviation of observations.
^eStandard deviation of simulations.
^fCorrelation coefficient between observation and simulation.

682 **Table 3** The number of haze days in February and July in Beijing. Also shown are the regional and temporal average
 683 surface wind speed (m s^{-1}), and visibility (km), relative humidity (%), as well as mass concentrations ($\mu\text{g m}^{-3}$) of sulfate,
 684 nitrate, ammonium, BC, OC, and $\text{PM}_{2.5}$ during the haze days in February and July, respectively, in Beijing.

variables	February	July
Number of haze days	7	13
Wind speed	3.13	3.41
Visibility	6.22	5.73
Relative humidity	55.80	74.32
Sulfate	37.99	52.32
Nitrate	54.78	48.37
Ammonium	30.15	33.60
BC	13.29	4.31
OC	19.51	5.16
$\text{PM}_{2.5}$	174.26	148.32

685
 686
 687
 688
 689
 690
 691
 692
 693
 694
 695
 696
 697
 698
 699
 700
 701
 702
 703
 704
 705
 706
 707
 708
 709
 710
 711
 712
 713
 714

715
716

717
718
719
720
721
722
723
724
725
726
727
728
729
730
731
732
733
734
735
736
737
738
739
740
741
742
743
744
745
746
747
748
749
750
751
752
753
754
755

Table 4 Regional and monthly average extinction contribution ratios (%) of sulfate, nitrate, ammonium, BC, OC, and other aerosols (dust, sea salt, and unspecified anthropogenic mass) in February and July, respectively, in Beijing.

	Sulfate	Nitrate	Ammonium	BC	OC	Others
Feb	22.73	29.69	17.13	5.05	13.22	12.18
Jul	39.31	24.77	21.88	0.33	3.96	9.74

756
757

758
759
760
761
762
763
764
765
766
767
768
769
770
771
772
773
774
775
776
777
778
779
780
781
782
783
784
785
786
787
788
789
790
791
792
793
794
795
796

Table 5 Regional and monthly average mass concentration threshold of PM_{2.5} (μg m⁻³) under different relative humidity from the sensitivity test in Beijing.

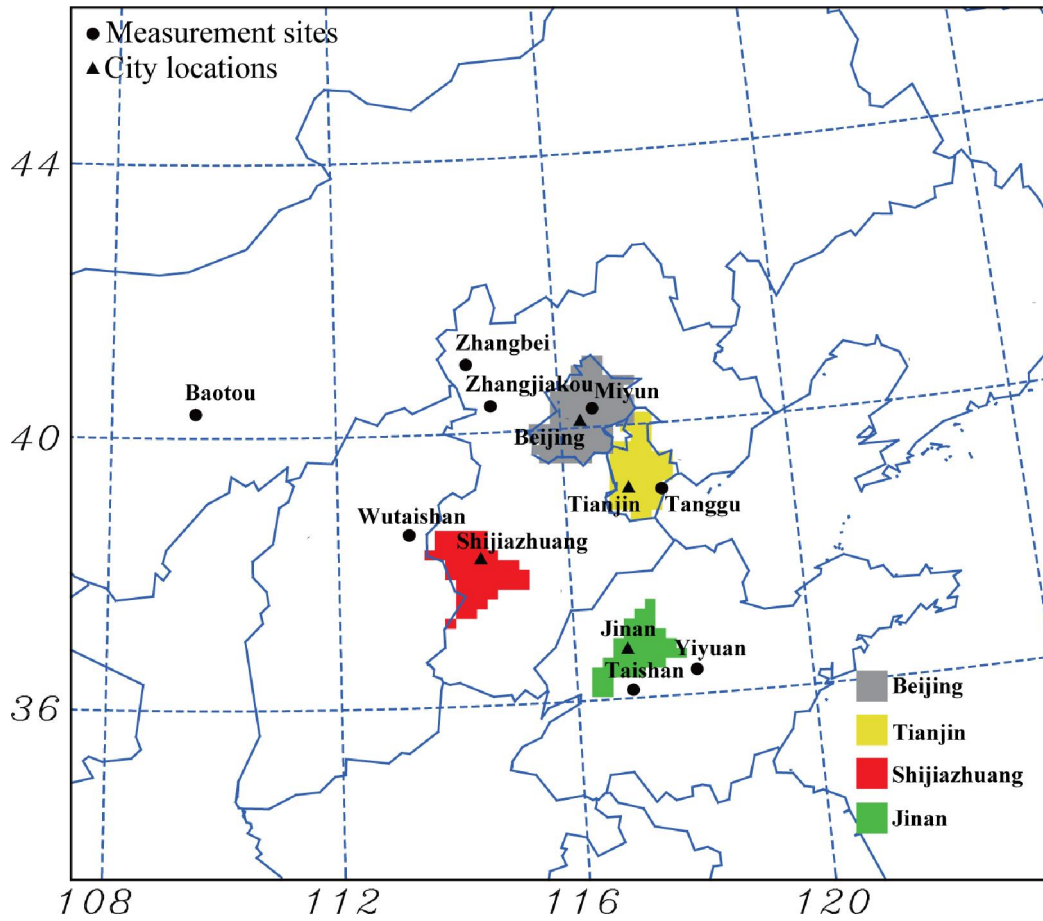
	70%	75%	80%	85%	88%	89%	90%
Feb	82.08	78.01	72.34	64.54	58.27	55.87	53.22
Jul	83.08	78.64	72.46	64.01	57.35	54.82	52.10

797
798

799
800
801
802
803
804
805
806
807
808
809
810
811
812
813
814
815
816
817
818
819
820
821
822
823
824
825
826
827

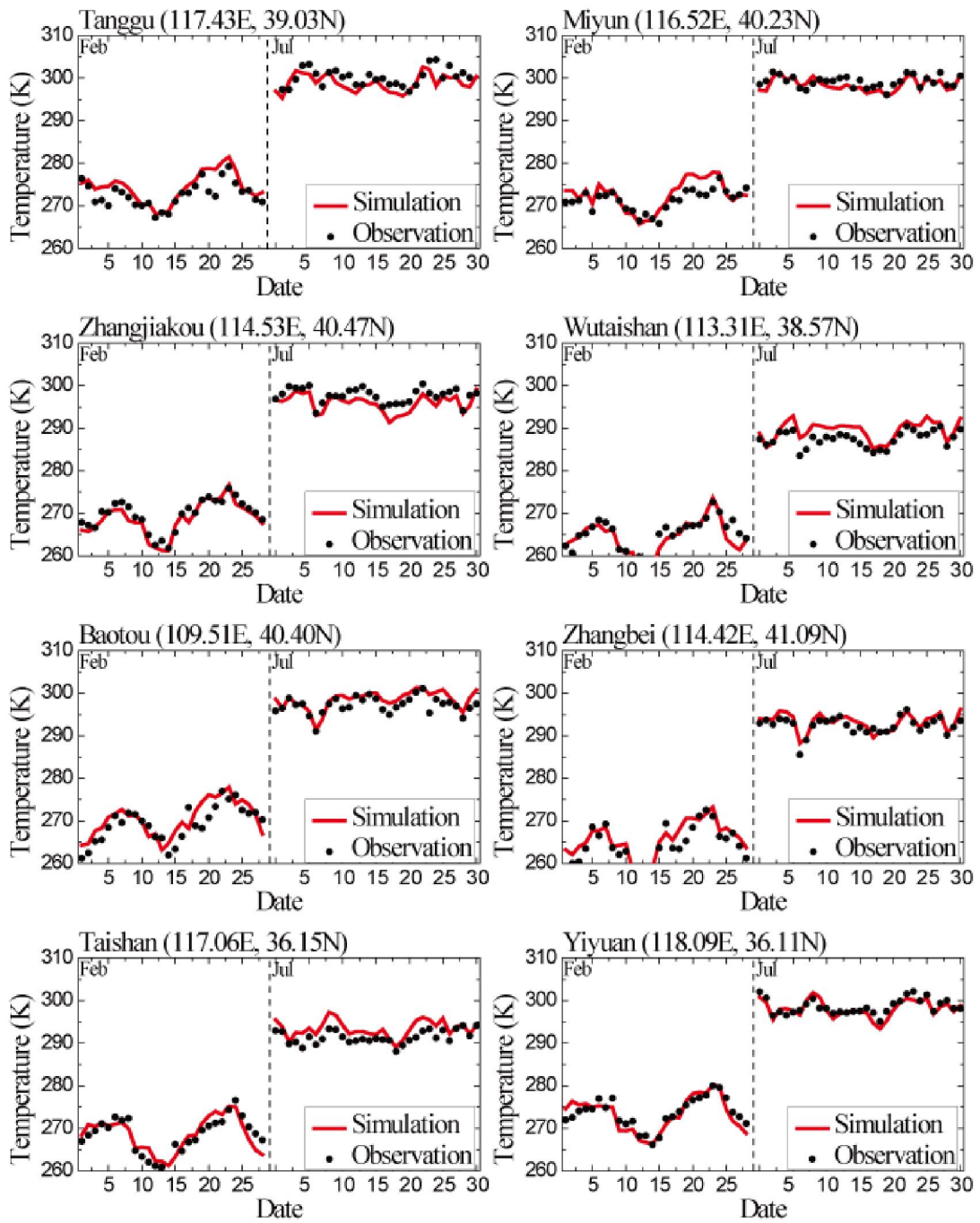
Table 6 Parameters of the exponential fit for regional and monthly average PM_{2.5} mass concentration threshold of haze occurrence in Beijing.

	<i>a</i>	<i>b</i>	<i>c</i>	R-square
Feb	96.3276	-0.4859	0.0486	0.9997
Jul	96.8810	0.7367	0.0483	0.9997



828
829
830
831
832
833
834
835
836
837
838
839
840
841
842
843

Fig. 1. Geographic location of API monitoring cities and CNMCM measurement stations in the model domain. The gray, yellow, red, and green areas represent the district of Beijing, Tianjin, Shijiazhuang, and Jinan, respectively.



844
845 **Fig. 2.** Observed (circle) and modeled (solid line) daily average temperature (K) at 8 stations in February and July 2011.

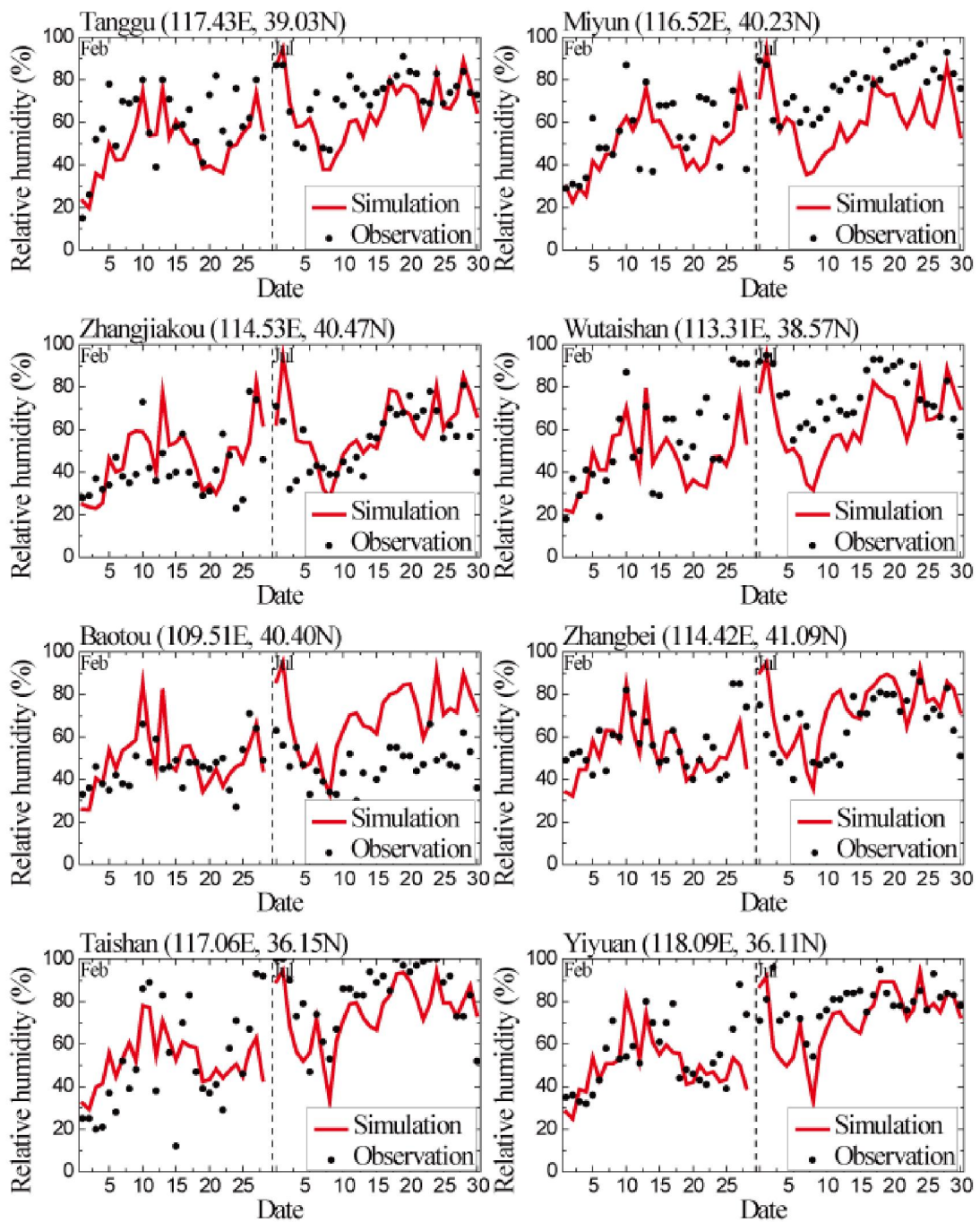


Fig. 3. Same as Fig. 2 but for relative humidity (%).

853
854
855
856
857
858
859
860
861

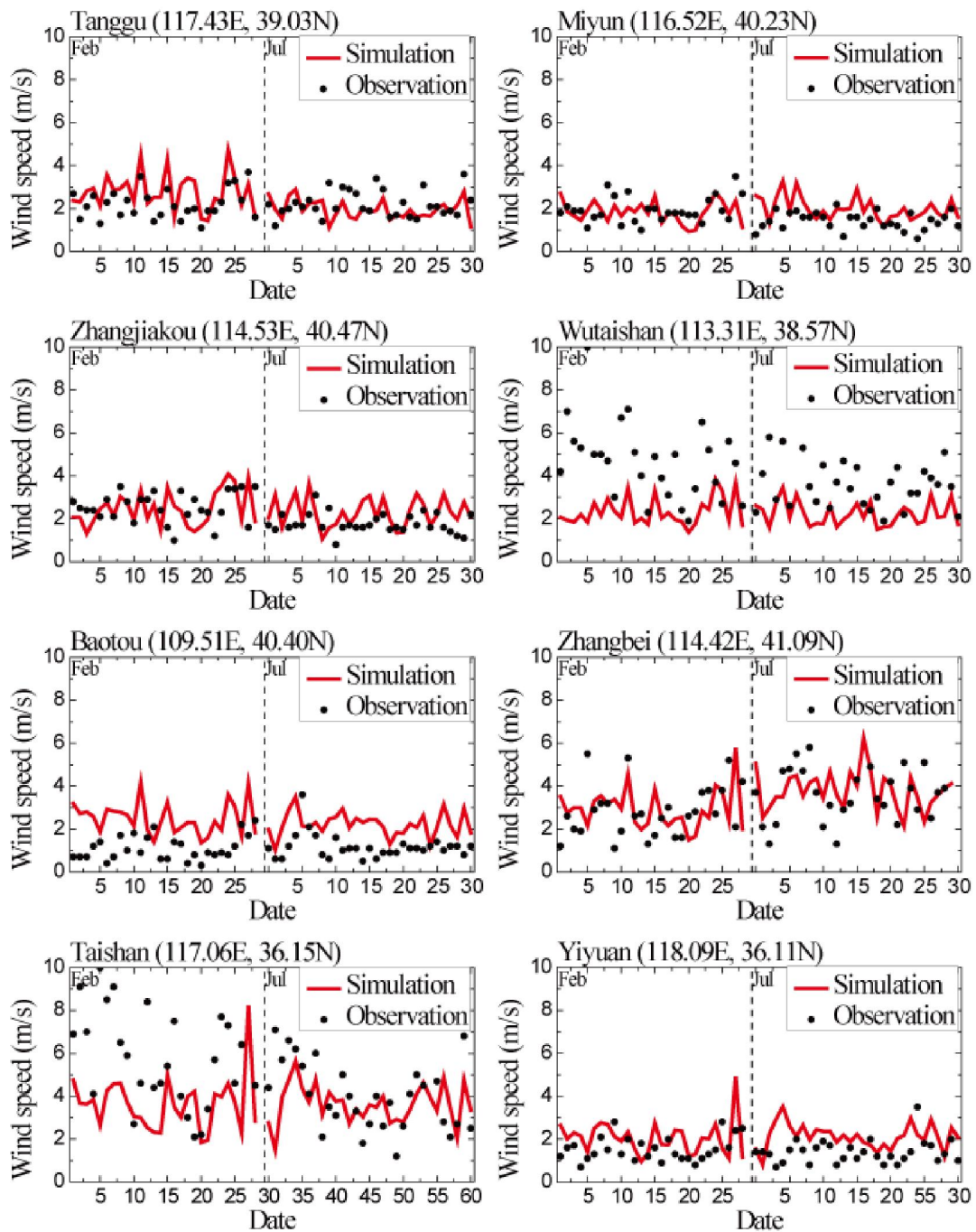


Fig. 4. Same as Fig. 2 but for wind speed (m s^{-1}).

862
863
864
865
866
867
868
869
870

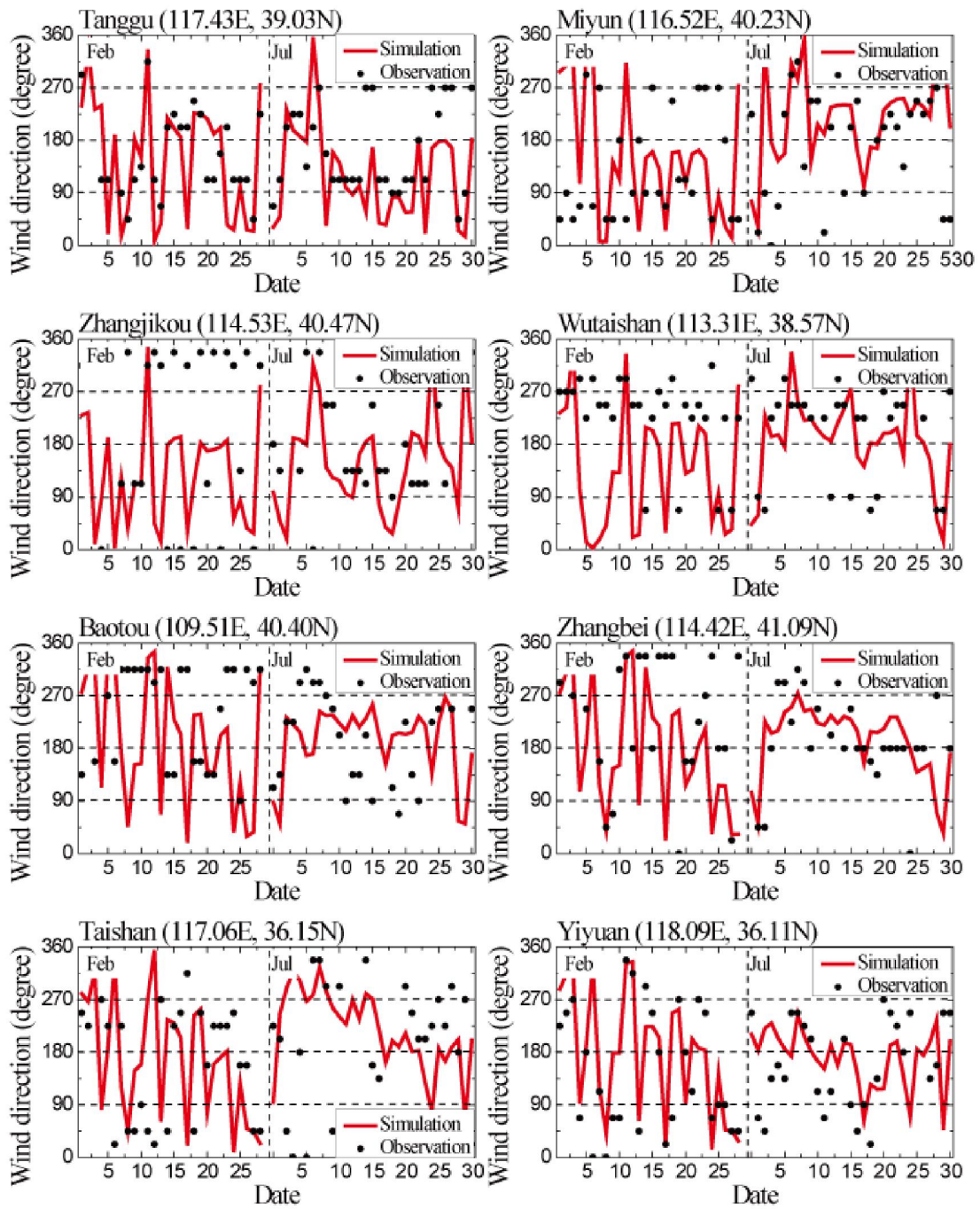


Fig. 5. Same as Fig. 2 but for wind direction (degree).

871
872
873
874
875
876
877
878
879

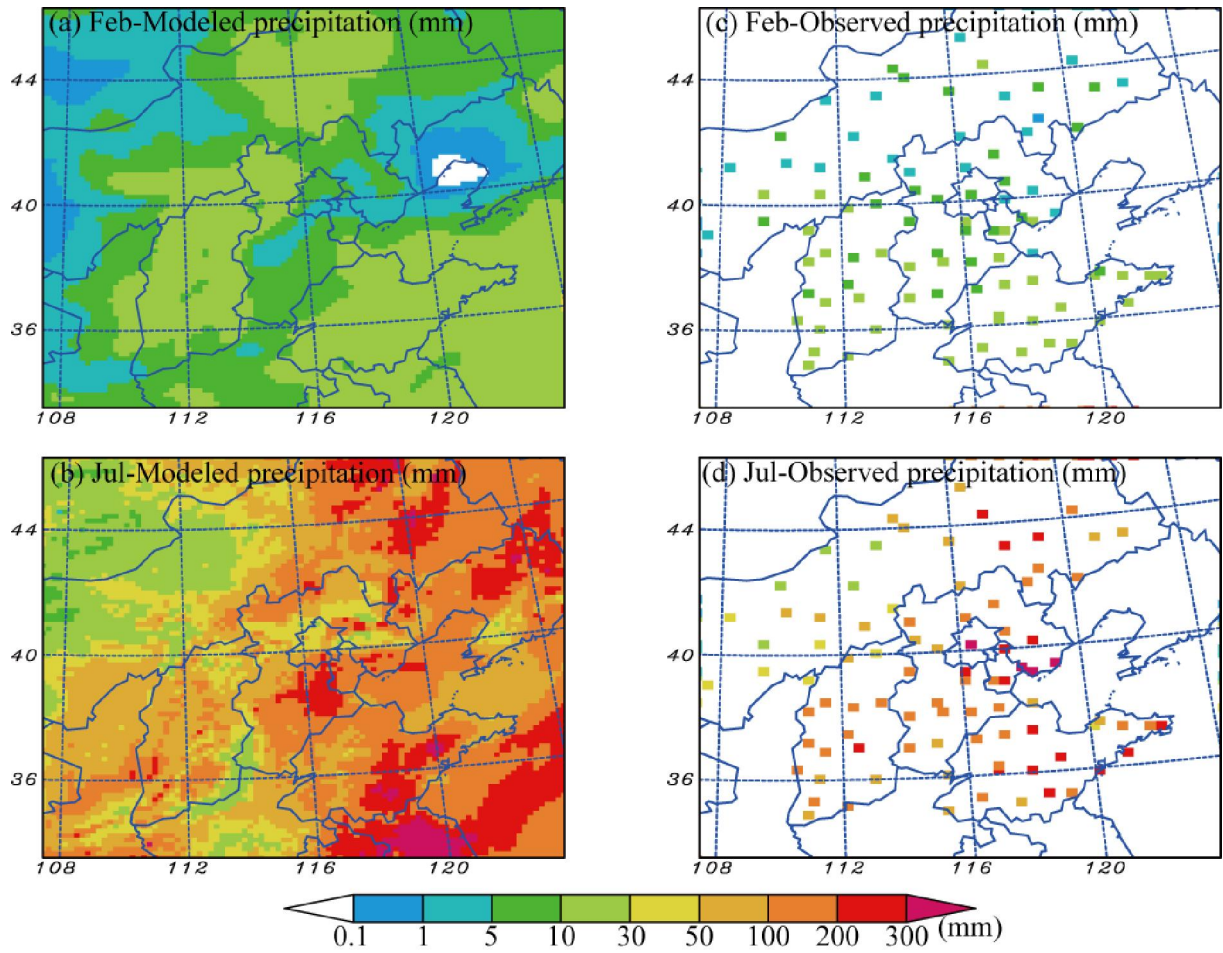
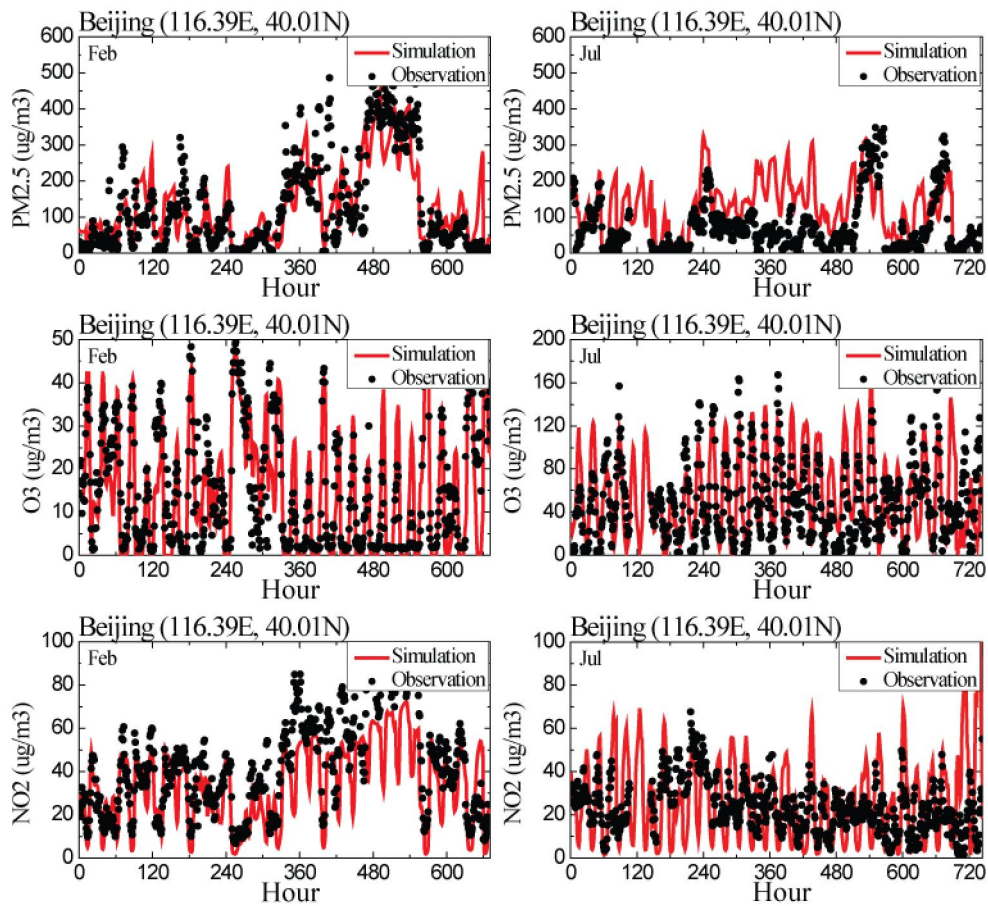


Fig. 6. The horizontal distributions of the monthly precipitation (mm) from simulation and surface observation data in February and July 2011 over NCP.



895
 896 **Fig. 7.** Observed (circle) and modeled (line) hourly mass concentrations ($\mu\text{g m}^{-3}$) of PM_{2.5}, O₃, and NO₂ in February and
 897 July 2011 at Beijing.
 898
 899
 900
 901
 902
 903
 904
 905
 906
 907
 908
 909
 910

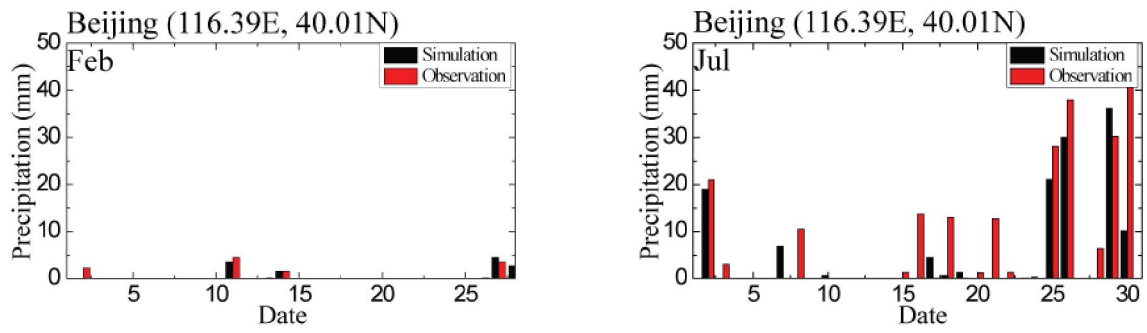


Fig. 8. Observed and modeled daily precipitation (mm) in February and July 2011 at Beijing

911
912
913
914
915
916
917
918
919
920
921
922
923
924
925
926
927
928
929
930
931
932
933
934
935

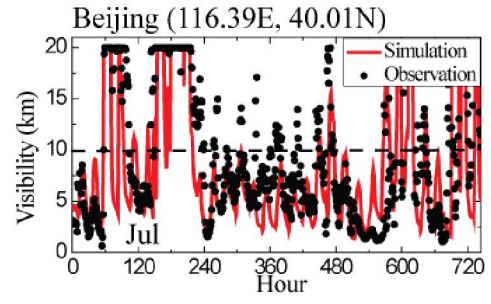
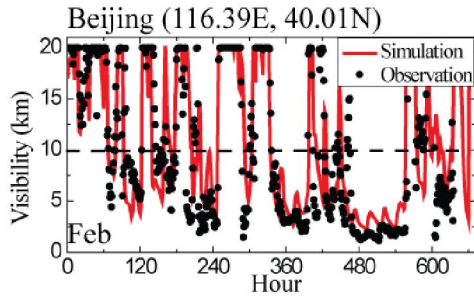


Fig. 9. Observed (circle) and modeled (line) hourly visibility (km) in February and July 2011 at Beijing.

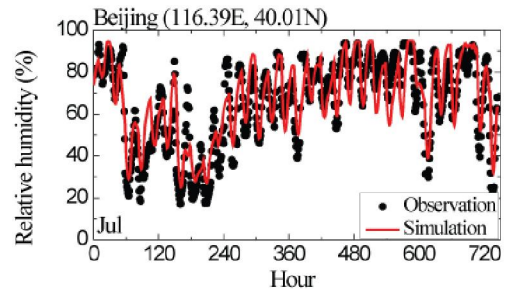
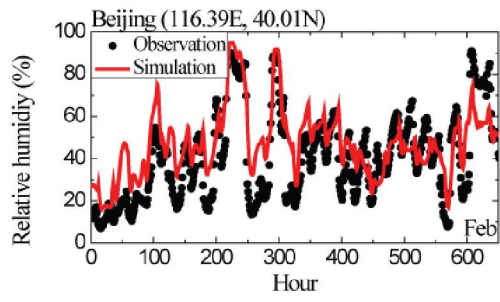
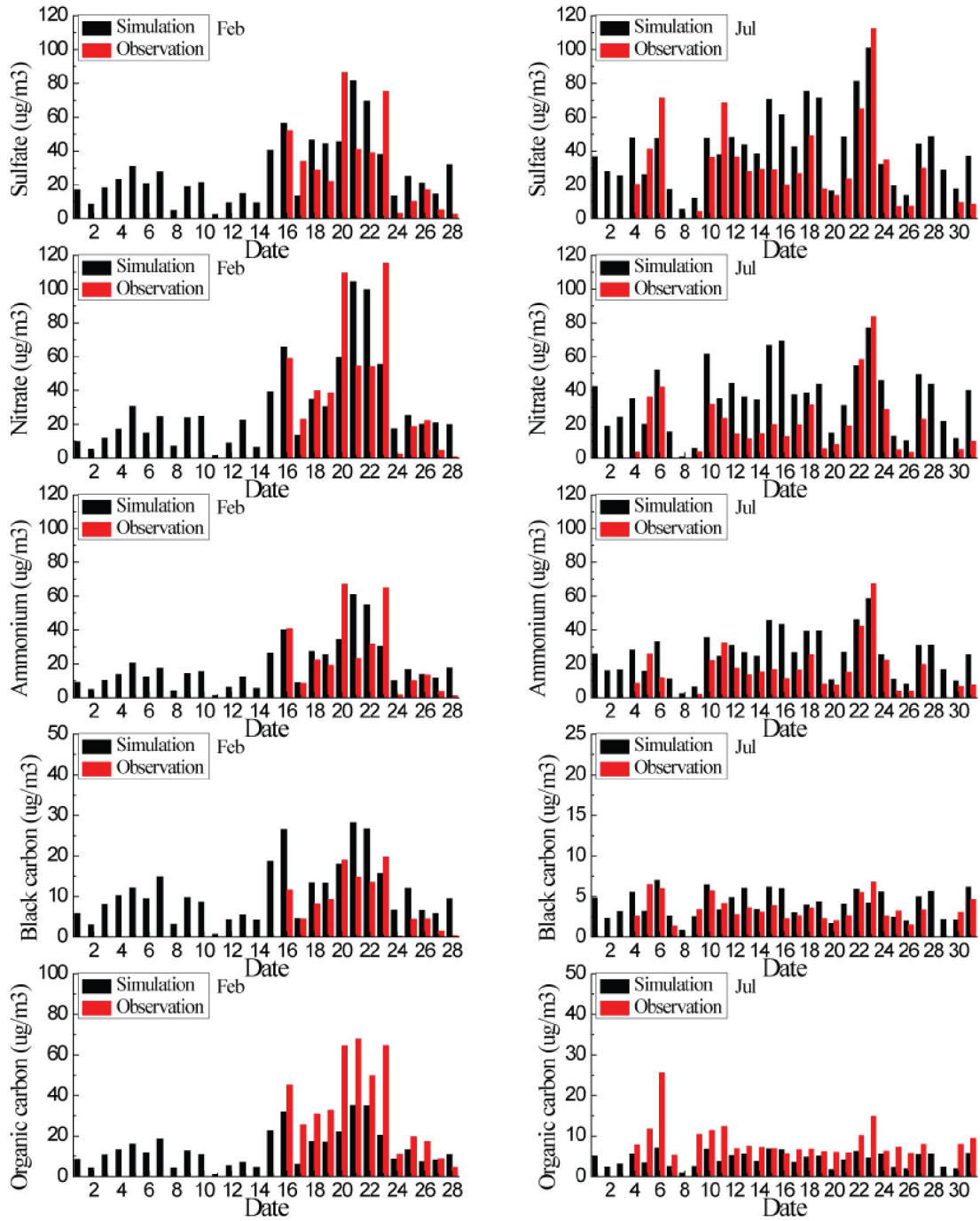
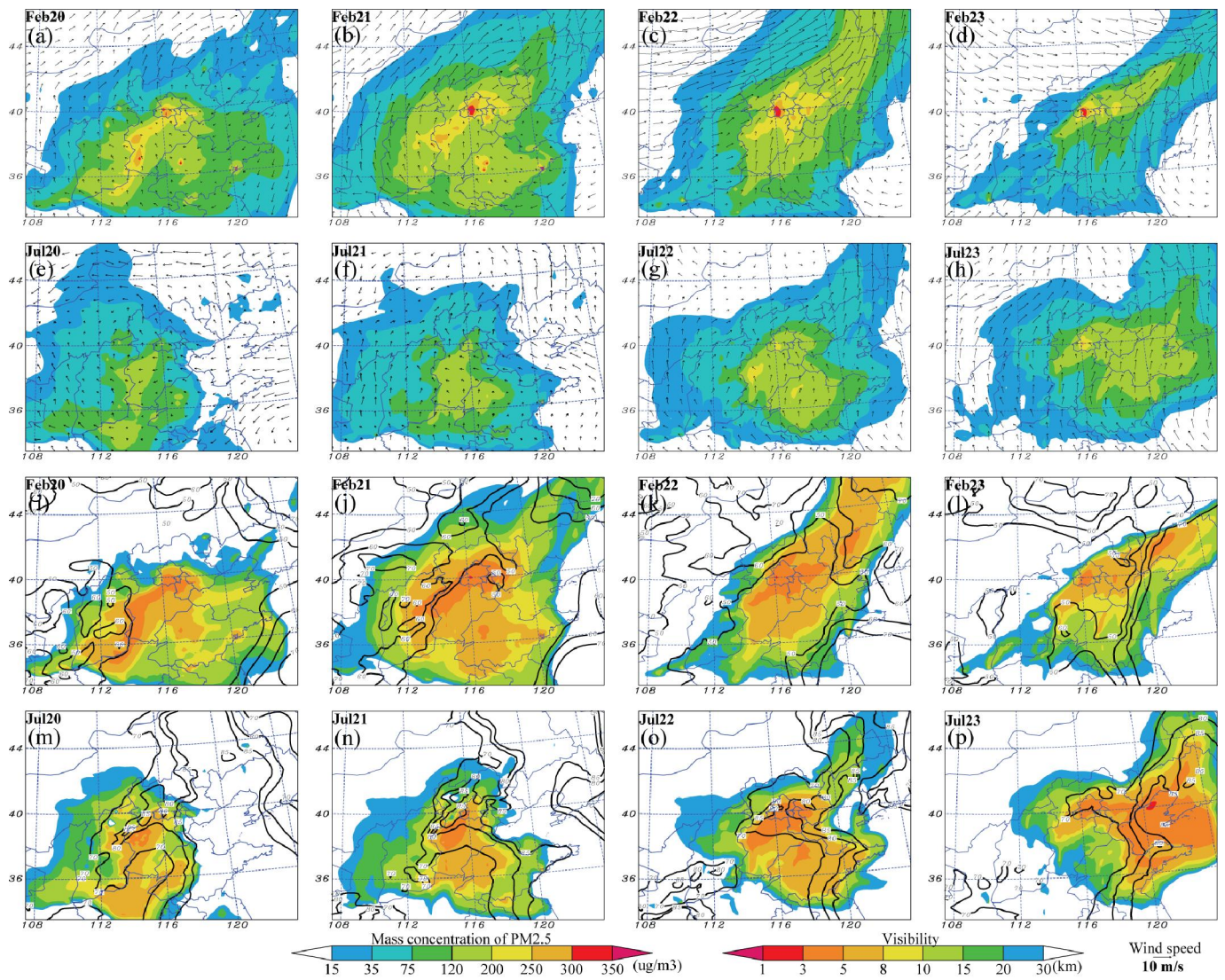


Fig. 10. Observed (circle) and modeled (line) hourly relative humidity (%) in February and July 2011 at Beijing.

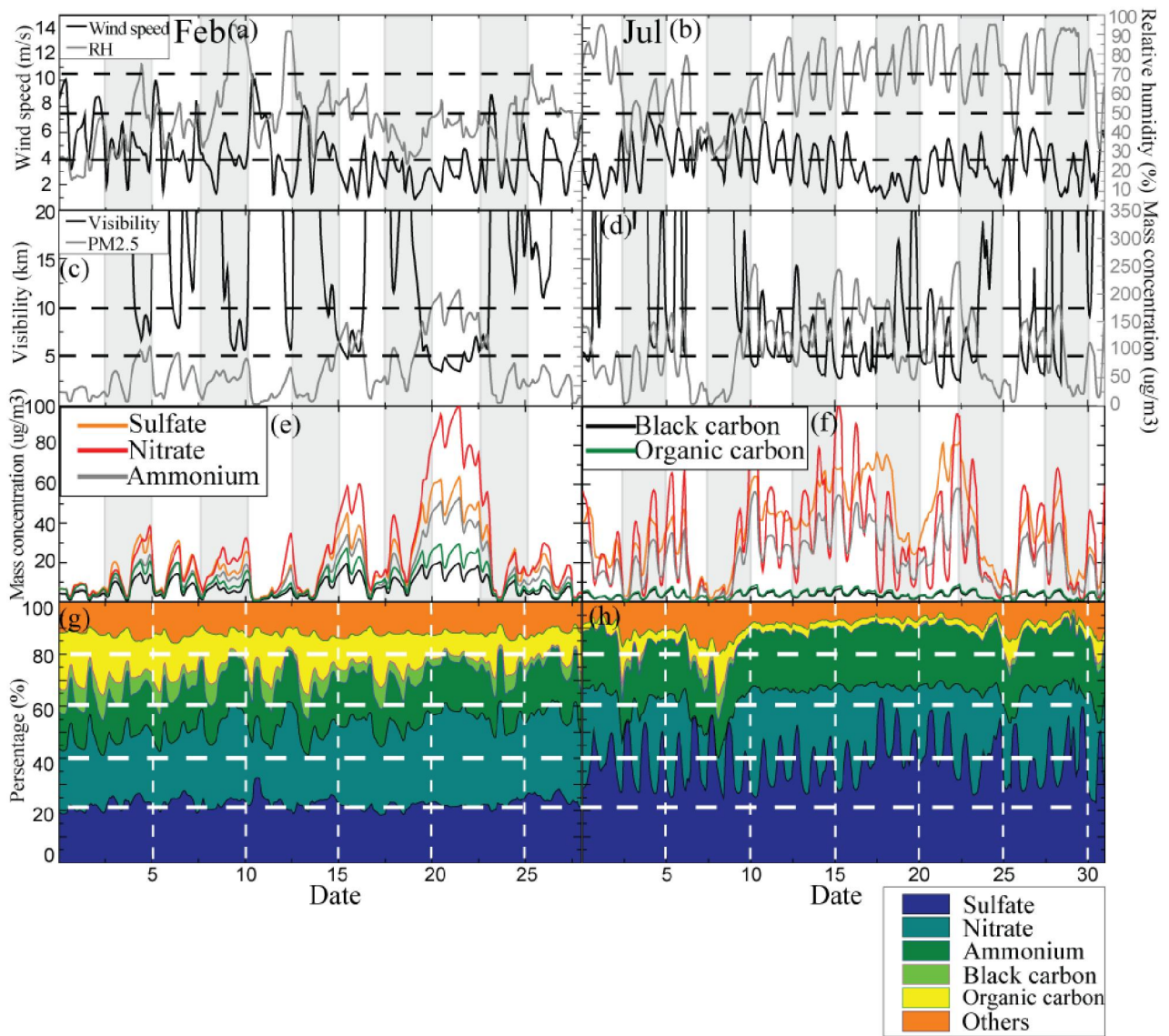
961
962
963
964
965
966
967
968
969
970
971
972
973
974
975
976
977
978
979
980
981
982
983
984
985



986
 987 **Fig. 11.** Observed (circle) and modeled (line) daily average mass concentrations ($\mu\text{g m}^{-3}$) of sulfate, nitrate, ammonium,
 988 black carbon, and organic carbon in February and July 2011 at Beijing.



994
 995 **Fig. 12.** The horizontal distributions of daily average mass concentration of PM_{2.5} ($\mu\text{g m}^{-3}$; a-h) and visibility (km; i-p)
 996 from February 20 to 23 and July 20 to 23 over NCP. Also shown is the wind field (arrows) and relative humidity (%;
 997 black contour lines).



1006
 1007 **Fig. 13.** The time series of regional average surface wind speed (m s^{-1}), and relative humidity (%), visibility (km), as
 1008 well as $\text{PM}_{2.5}$ mass concentrations ($\mu\text{g m}^{-3}$) in February and July in Beijing (a-d). Also shown are the mass concentrations
 1009 ($\mu\text{g m}^{-3}$; e-f) and extinction contribution ratios (g-h) of sulfate, nitrate, ammonium, BC, OC, and other aerosols (dust, sea
 1010 salt, and unspecified anthropogenic mass).

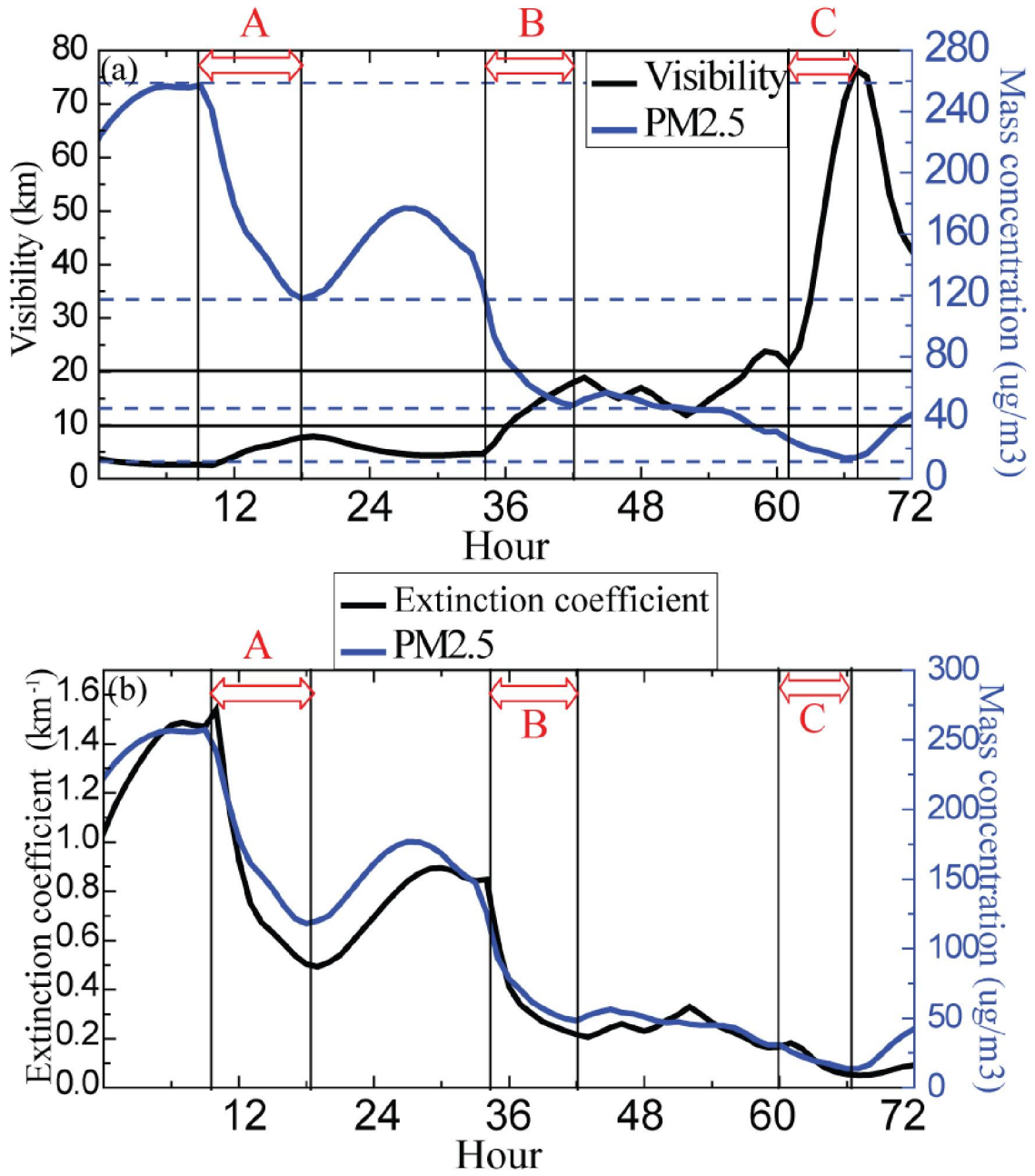
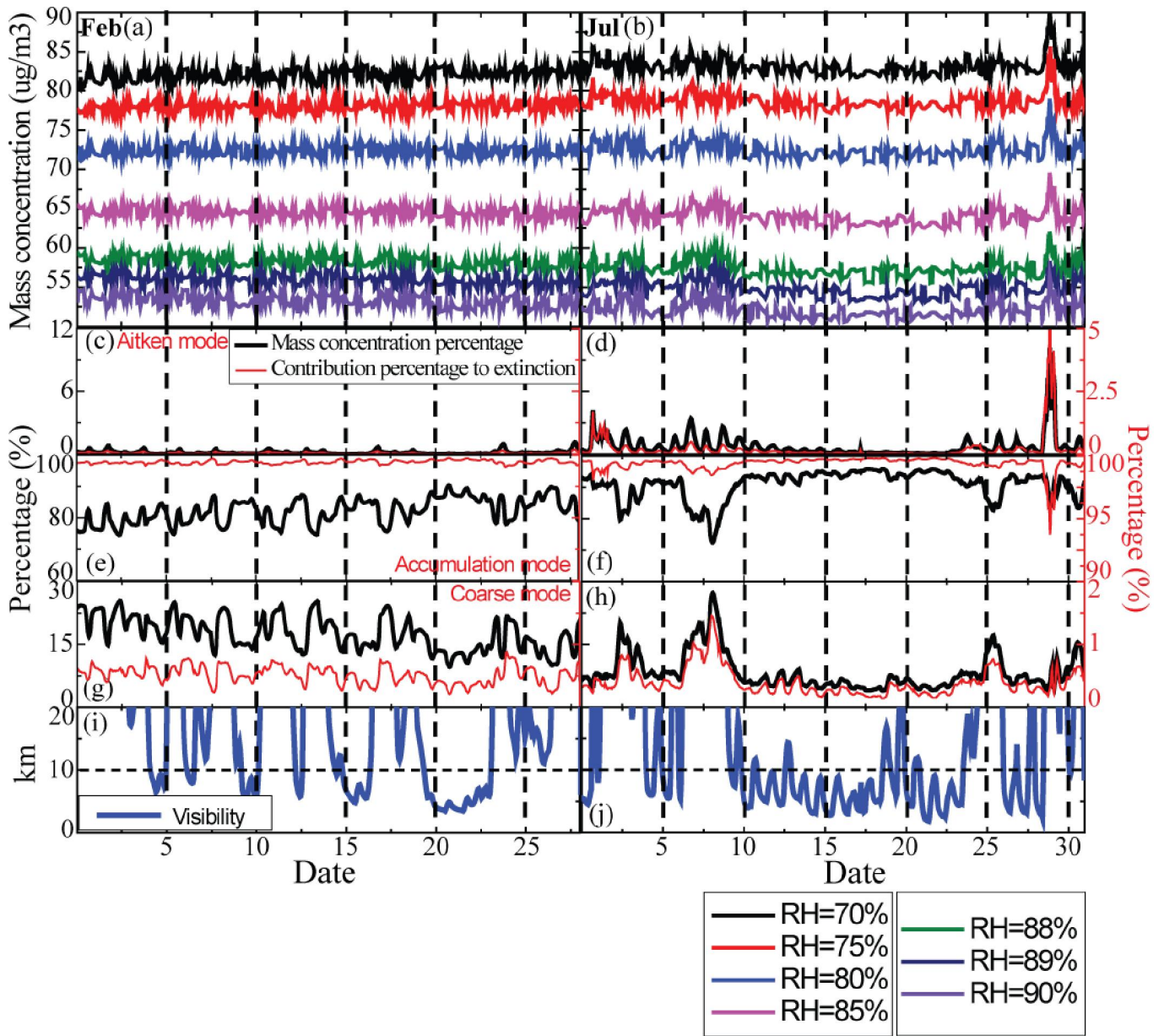


Fig. 14. The time series of regional average visibility (km) vs. mass concentration of PM_{2.5} (a), and extinction coefficient vs. mass concentration of PM_{2.5} (b) from July 23 to 25 in Beijing.

1017
 1018
 1019
 1020
 1021
 1022
 1023
 1024
 1025



1026
 1027 **Fig. 15.** The time series of regional average mass concentration threshold of $PM_{2.5}$ under different relative humidity (%)
 1028 from the sensitivity test in February and July in Beijing. Also shown are the mass ratios and extinction contribution ratios
 1029 (%) of Aitken mode, accumulation mode, and coarse mode, and visibility (km).
 1030
 1031
 1032
 1033
 1034
 1035
 1036

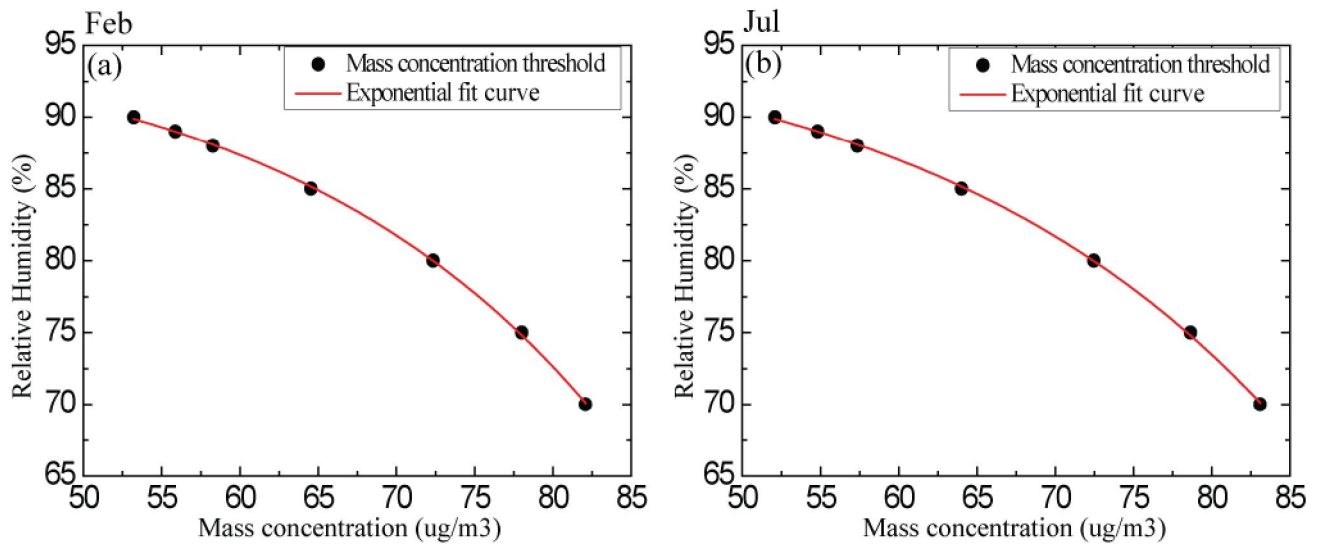


Fig. 16. The relationship between regional and monthly average PM_{2.5} mass concentration threshold of haze occurrence and relative humidity in Beijing. Also shown are the exponential fit curves of the data.

1037
 1038
 1039
 1040
 1041
 1042
 1043
 1044